



UNIVERSITY OF LEEDS

This is a repository copy of *Fractional robust finite time control of four-wheel-steering mobile robots subject to serious time-varying perturbations*.

White Rose Research Online URL for this paper:

<https://eprints.whiterose.ac.uk/182100/>

Version: Accepted Version

Article:

Jiang, L, Wang, S, Xie, Y et al. (3 more authors) (2022) Fractional robust finite time control of four-wheel-steering mobile robots subject to serious time-varying perturbations.

Mechanism and Machine Theory, 169. 104634. ISSN 0094-114X

<https://doi.org/10.1016/j.mechmachtheory.2021.104634>

© 2021, Elsevier. This manuscript version is made available under the CC-BY-NC-ND 4.0 license <http://creativecommons.org/licenses/by-nc-nd/4.0/>.

Reuse

This article is distributed under the terms of the Creative Commons Attribution-NonCommercial-NoDerivs (CC BY-NC-ND) licence. This licence only allows you to download this work and share it with others as long as you credit the authors, but you can't change the article in any way or use it commercially. More information and the full terms of the licence here: <https://creativecommons.org/licenses/>

Takedown

If you consider content in White Rose Research Online to be in breach of UK law, please notify us by emailing eprints@whiterose.ac.uk including the URL of the record and the reason for the withdrawal request.



eprints@whiterose.ac.uk
<https://eprints.whiterose.ac.uk/>

1 Fractional Robust Finite Time Control of Four-wheel-steering Mobile Robots 2 Subject to Serious Time-varying Perturbations

3 Liquan Jiang^a, Shuting Wang^a, Yuanlong Xie^{a*}, Sheng Quan Xie^{b,c}, Shiqi Zheng^d, Jie Meng^a

4 ^a School of Mechanical Science and Engineering, Huazhong University of Science and Technology,
5 1037 Luoyu Road, Wuhan 430074, China

6 ^b School of Electronic and Electrical Engineering, University of Leeds, Leeds LS2 9JT, UK

7 ^c Institute of Rehabilitation Engineering, Binzhou Medical University, Yantai 264033, China

8 ^d School of Automation, China University of Geosciences, 388 Lumo Road, Wuhan 430074, China

9 * Corresponding author: Yuanlong Xie

10 * Email: yuanlongxie@hust.edu.cn

11 * Phone: +86-15927427952

12 Abstract:

13 The four-wheel-steering mobile robot (FMR) is widely applied in the manufacturing industry,
14 where accurate and stable lateral motion control is a prerequisite for ensuring manufacturing quality
15 and efficiency. However, serious time-varying perturbations such as system uncertainties and external
16 disturbances usually lead to unsatisfactory control performance. By designing constrained prediction
17 and sliding mode mechanisms, a novel adaptive fractional robust finite time controller is proposed to
18 achieve a system with required control accuracy and stability under serious time-varying perturbations.
19 Compared with existing FMR solutions, the proposed method has the following attractive properties: 1)
20 Without requiring the derivatives of time-varying perturbations, the proposed method utilizes a modi-
21 fied fractional super-twisting sliding mode switching law to guarantee the system robustness of dy-
22 namical tracking and disturbance rejection; 2) The differences between the nominal predicted states and
23 the feedback ones can be well accommodated despite unmodeled dynamics and external disturbance; 3)
24 By designing continuous control inputs, the “chattering phenomenon” in conventional control laws is
25 carefully handled. Moreover, sufficient conditions are derived for the variable control gains to ensure
26 the input-to-state practical stability and finite time convergence. Under harsh working conditions, two
27 comparative experiments implemented on a real-life FRM are performed for demonstrative purposes.

28 Keywords:

29 four-wheel-steering mobile robots, fractional robust finite time control, time-varying perturbations,
30 sliding mode mechanism

Nomenclature

β	Sideslip angle, <i>rad</i>
γ	Yaw rate, <i>rad/s</i>
v_x	Longitude velocity, <i>m/s</i>
m	Total mass, <i>kg</i>
C_f	Lateral stiffness of the front wheel, <i>N/rad</i>
C_r	Lateral stiffness of the rear wheel, <i>N/rad</i>
I_z	Inertia moment, <i>kg m²</i>
L	Length between front axle and rear axle, <i>m</i>
L_f	Length from the front axle to the center of the mass, <i>m</i>
L_r	Length from the rear axle to the center of the mass, <i>m</i>
δ_f	Steering angle of the front wheel, <i>rad</i>
M_Z	Yaw moment, <i>Nm</i>
$\sum F_x$	Total driving force of the four-wheel motors, <i>N</i>
T	Sampling time, <i>s</i>
$\eta_{i=1,2}$	Control gains
M	Upper boundary of the lumped perturbations
$\tilde{n}_{i=1,2}, \kappa, \delta, \mu, k_f$	Control parameters
α	Fractional order
$f_{i=1,2,3}$	Unknown perturbations
s	Sliding mode surface
Υ	Disturbance boundary
$u(t)$	Control law
$u_{NMPC}(t)$	Nominal control law

$v(t)$	Super-twisting-based control law
T, Q	Weight matrices
N_c	Control horizon
N_p	Prediction horizon
K_g	Control gain
O_o	Infeasible region
O_f	Obstacle-free space

1. Introduction

Recently, mobile robots have been crucially applied in industrial scenarios such as manufacturing plants and logistics transportation [1-5]. Different from differential wheels, the mobile robot actuated by Mecanum wheels has the potential in constrained or confined environments. This is because it can achieve an arbitrary effective movement [6,7]. The disadvantage of the Mecanum wheel lies in its poor locomotive efficiency because not all the wheels rotate in the direction of movement [8]. This disadvantage also causes loss from ground friction interaction. In comparison, actuated by in-wheel or hub motors, a four-wheel-steering mobile robot (FMR) can perform lateral motion in an arbitrary orientation. It has better adaptability on complex ground conditions or high maneuverability required in confined spaces. Although the FMR has increased popularity in modern industrial applications, serious time-varying perturbations, including parametric variations, structured or unstructured uncertainties, and external disturbances may affect the trajectory tracking precision [9]. In addition, scholars found that the chassis of the mobile robot system shows evident fractional order features [10]. Compared with integer order system, fractional order controller introduces additional degrees of freedom. This enables the controlled integral or fractional systems to achieve superior performance and enhanced robustness of the system [11]. The application of fractional order controllers is an important supplement to the control fields of the mobile robot [12,13]. Due to the theoretical and practical significances, accurate and robust FMR systems have become an inseparable part that deserves deep exploration in the control fields during the last decades [14-17].

The tracking operation of the mobile robot can be realized by using simple kinematic solutions [18,19]. However, this method does not pay attention to the motion actuation mechanism. The dynamic characteristics of the system are easy to be affected in the external complex scene, such as uneven ground and slippery roads. By contrast, the accurate dynamic adjustment of the mobile robot chassis can be realized through dynamic control to improve the tracking performance [20-22]. As a widely employed control strategy, direct yaw moment control (DYMC) framework establishes the relationship between robot motion, driving force and yaw moment [23]. It has an excellent ability in stability control and tracking accuracy, which has attracted extensive attention in industrial FMR implementation. Moreover, the cornering stability can be improved through the control strategy based on DYMC. This is realized by using the wheel angle information and the traction force between the left and right wheels. DYMC adjusts torque-vectoring differential or separately controlled motor to improve the movement stability and efficiency. Up to now, various studies have focused on DYMC to enhance the anti-interference and robust tracking ability of FMR [24-26]. For instance, the concurrent control of yaw rate and sideslip angle was studied in the frequency domain to satisfy the vehicle handling requirements [27]. To strengthen the lateral stability and path tracking performance, a hierarchical control method was proposed by integrating a coordinated path following system and DYMC for autonomous electric vehicles [9]. However, most of the above studies are focused on the DYMC system with asymptotic convergence, which may not offer sufficient robustness against serious perturbations of FMR systems in critical operating situations.

For practical implementations of FMR systems, finite time control (FTC) with an adaptive framework has attracted increasing attention nowadays [28,29]. Compared to asymptotic control methods, FTC or fixed time control can ensure the convergence of the system within finite time. The FTC has the inherent advantages of achieving stronger robustness against unknown disturbances than traditional asymptotic schemes. Moreover, it has the potential for decoupling the closed-loop stabilization or tracking control objective from the others. For mobile robot applications, the effort has been placed towards deriving FTC strategies, such as adaptive robust control [30], sliding mode control (SMC) [31], and backstepping control [32]. Now, SMC has shown outstanding advantages in handling system uncertainties in industrial fields [33-36]. For example, to achieve image-based visual servo of the wheeled mobile robot system, a novel fuzzy integral SMC method was proposed to eliminate the reaching phase while improving the transient performance [37]. In [38], a practical second-order SMC technique was applied to compensate for the friction effect of a mobile robot. This method does not require any explicit friction model with a low calculation burden. However, the existence of chattering

1 restricts the performance of SMC. By driving the sliding mode and its derivatives near zero, high-order
2 sliding mode control is effective to alleviate chattering caused by traditional SMC control methods [39].
3 Thus, the system robustness and control accuracy can be improved. Nevertheless, high-order sliding
4 mode has higher requirements for external disturbance boundary value. How to use the high-order de-
5 rivative of the sliding variable is one of the remaining problems. In comparison, variable gain control
6 can be one of the effective methods to improve the anti-disturbance ability and alleviate the chattering
7 simultaneously [40]. However, a reasonable gain value and its adjustment rules still need further ex-
8 ploration. Thus, as a powerful second-order SMC, the variable gain super-twisting SMC is applicable
9 to systems subject to lump bounded disturbances. The required sliding motion can be realized by de-
10 signing an appropriate control mechanism to increase stabilization, accuracy, and convergence. Without
11 differentiating a sliding variable, the super-twisting SMC can achieve strengthened convergence, re-
12 duced chattering, lower sensitivity to system parameter variations and disturbances.

13 Even though SMC has the above-mentioned attractive merits, serious time-varying perturbations
14 must be carefully addressed to stabilize the concerned FMR system [41, 42]. The intuitive reason is that
15 undesirable perturbations may cause an undesirable situation if the resulting controllers are not suffi-
16 ciently robust, which then naturally cause oscillations or vibrations [43, 44]. The mentioned SMC de-
17 signs have in common that the constructed sliding variable is driven to a small neighborhood of the
18 origin and kept there regardless of the disturbances' behavior. This is achieved by assuming the upper
19 boundary of the uncertainties and the corresponding derivative to be pre-known [45-47]. Under this
20 circumstance, the closed-loop performance of the achieved controller can become independent of seri-
21 ous perturbations. However, because the uncertainties cannot be directly reflected in the control gains,
22 large control gains should be selected to enhance system robustness, which may lead to the gain over-
23 estimation and serious chattering phenomena. To the best of our knowledge, limited work has been
24 conducted on FTC integrated with the DYMC framework for the FMR system subject to serious
25 time-varying perturbations. Thus, this paper aims to solve the following open-questions to improve the
26 control capabilities of FMR systems: 1) how to deal with the time-varying unknown perturbations ro-
27 bustly to achieve a resultant system with reduced uncertainty because several strict conditions (e.g.
28 upper boundaries of the disturbances and related derivatives need to be acquirable) must be satisfied, 2)
29 how to design a nominal controller and a continuous SMC to achieve the finite time scheme while ful-
30 filling state and input constraints and canceling out the unknown perturbations and 3) how to address
31 the "chattering phenomenon" without overestimating the related control gains because the chattering
32 issue of the traditional discontinuous SMC may not be effectively addressed.

33 Consequently, an effective fractional robust finite-time control (FRFTC) method is developed for
34 the FMR system. Under this method, the required closed-loop stability can be guaranteed under serious
35 lump time-varying perturbations (such as the unmodeled dynamics and parametric vibrations). Com-
36 pared with the traditional control solutions used in FMR (such as [48-50]), the main contributions are
37 as follows: 1) By designing a fractional-order variable gain adaption mechanism, the proposed method
38 can directly suppress the complex disturbance without requiring the upper boundary or correlation de-
39 rivatives of the disturbances. In this manner, the balance between the trajectory tracking accuracy and
40 anti-disturbance accruing in traditional methods [47] can be avoided. 2) An improved super-twisting
41 like SMC is realized to seek continuous control inputs such that control chattering in [33,38] is carefully
42 eliminated, and the undesirable chattering caused by high control gain of conventional SMC solutions
43 can be prevented [45]. 3) Combined with piecewise nonlinear model predictive control (NMPC), the
44 proposed method provides the necessary conditions for the system state to converge to a small region.
45 In this way, the closed-loop stability and finite time convergence of the FMR system can be guaranteed.
46 4) The adaptive FRFTC control scheme is verified on the developed platform. The DYMC scheme is
47 used to adjust the lateral motion advantages to adapt to different environmental conditions.

48 The remaining portion is structured as follows: The problem statements are provided in Section II.
49 Detailed design procedures of the proposed FRFTC method with input-to-state practical stability and
50 convergence analyses are discussed in Section III. Experimental examples are provided in Section IV.
51 Several concluding discussions and future works are presented in Section V.

52 *Notations:* In this paper, \mathbb{R}^+ is the set of nonnegative real numbers, \mathbb{R}^n is the n -dimensional
53 Euclidean space, $\|\cdot\|$ is the standard Euclidean norm, \star is asymmetric element of matrix, and
54 $\lambda_{\max}(\cdot)$ and $\lambda_{\min}(\cdot)$ are the maximum and minimum eigenvalues of any symmetric matrix \cdot , re-
55 spectively. The notation $\|x\|^\gamma$ denotes x and γ in \mathbb{R} with $\gamma \geq 0$ to denote $|x|^\gamma \text{sign}(x)$.

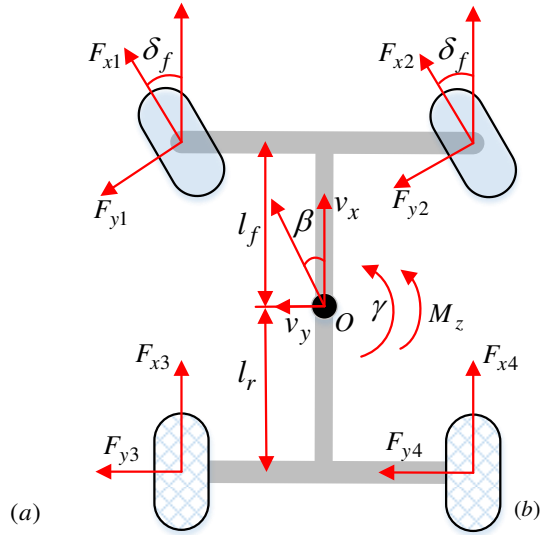


Fig. 1 Considered FMR system: (a) Developed prototype, (b) Four-wheel model.

2. System Modeling and Problem Formulation

2.1 FMR System Modeling

The concerned FMR is a nonlinear system with interconnected states under the lateral motion control framework [51, 52]. With two virtual front and rear wheels, the FMR dynamics in Fig. 1 (b) is determined by

$$\begin{aligned}\dot{\beta} &= \frac{C_f + C_r}{mv_x} \beta + \left(\frac{L_f C_f - L_r C_r}{mv_x^2} - 1 \right) \gamma - \frac{C_f}{mv_x} \delta_f + f_1 \\ \dot{\gamma} &= \frac{L_f C_f - L_r C_r}{I_z} \beta + \frac{L_f^2 C_f + L_r^2 C_r}{I_z v_x} \gamma - \frac{L_f C_f}{I_z} \delta_f + \frac{M_z}{I_z} + f_2 \\ \dot{v}_x &= \beta \gamma v_x - \frac{C_f}{m} \left(\beta + \frac{L_f}{v_c} \gamma \right) \delta_f + \frac{1}{m} \sum F_x + f_3\end{aligned}\quad (1)$$

where β , γ and v_x are the sideslip angle, yaw rate and longitude velocity, separately; m is the total mass; C_f and C_r are the lateral stiffness of front wheel and rear wheel, respectively; I_z is the inertia moment; L_f and L_r are the related lengths shown in Fig. 1; δ_f is the steering angle of the front wheel; M_z is the yaw moment; f_1 , f_2 and f_3 are the unknown perturbations, including the parametric uncertainties, road interferences and external disturbances; $\sum F_x$ is the total driving force of the four-wheeled motors, which can be determined by

$$\sum F_x = -\sum_{i=1}^4 \frac{T_i}{R_i}$$

where T_i denotes the driving torque of the i th motor, and R_i denotes the radius of the i th wheel.

As presented in [53], the reference value of γ and β can be described as follows:

$$\gamma_d = \frac{1}{1 + \left(\frac{L_f C_f - L_r C_r}{C_f C_r} \right) \frac{m}{L^2} v_x^2} \frac{v_x}{L} \delta_f, \quad \beta_d = \frac{1 - \left(\frac{m}{L} \right) \left(\frac{L_f}{L_r C_r} \right) v_x^2}{1 + \left(\frac{L_f C_f - L_r C_r}{C_f C_r} \right) \frac{m}{L^2} v_x^2} \frac{L_r}{L} \delta_f$$

Denote $x(t)$ and $u(t)$ as the system state and the control law vectors, respectively. The FMR system subject to unmatched perturbations is reformulated as

$$\dot{x}(t) = A(x(t)) + B(x(t))u(t) + f(x(t), t) \quad (2)$$

with

$$1 \quad A(x(t)) = \begin{bmatrix} \frac{C_f + C_r}{mv_x} & \left(\frac{L_f C_f - L_r C_r}{mv_x^2} - 1 \right) & 0 \\ \frac{L_f C_f - L_r C_r}{I_z} & \frac{L_f^2 C_f + L_r^2 C_r}{I_z v_x} & 0 \\ 0 & 0 & \beta\gamma \end{bmatrix} x(t), \quad B(x(t)) = \begin{bmatrix} -\frac{C_f}{mv_x} & 0 & 0 \\ -\frac{L_f C_f}{I_z} & \frac{1}{I_z} & 0 \\ -\frac{C_f}{m} \left(\beta + \frac{L_f}{v_c} \gamma \right) & 0 & \frac{1}{m} \end{bmatrix}$$

2 where $x(t) = [\beta, \gamma, v_x]^T$, $u(t) = [\delta_f, M_z, \sum F_x]^T$. $f(x(t), t) = [f_1 \ f_2 \ f_3]$ are the additive lump
3 perturbations due to the external environment, dynamic perturbation between the real physical model
4 and its nominal states with respect to $A(x(t))$ and $B(x(t))u(t)$.

5 **Remark 1.** As studied in [24], [25], the fixed longitudinal speed v_x is used in the existing modeling
6 methods. Thus, a simplified 2-DOF lateral dynamic model can be established to reduce the modeling
7 complexity. However, a constant longitudinal speed is difficult to keep in practice due to the dynamic
8 environment. Moreover, kinematics states in terms of longitudinal, lateral, and angular positions in the
9 inertial frame are introduced in [15]. Second-order derivatives of kinematics states can be considered as
10 the correspondence of the state variables β , γ and v_x here [23]. In the inertial coordinate system,
11 the absolute displacement offset is difficult to measure and not conducive to the practical implementa-
12 tion of the considered FMR. In comparison, the modeling framework based on DYMC compensates for
13 the steering input with yaw moment generated by longitudinal tire force. This can accommodate the
14 longitudinal-lateral motion of the FMR in different scenarios. Moreover, longitudinal speed v_x is intro-
15 duced in this paper to establish a 3-DOF lateral dynamic model. As compared with the traditional
16 2-DOF model [7], [8], the modeling accuracy is further improved.

17 2.2 Control Problem and Objective Formulation

18 *Control problem:* Under serious perturbations, an optimal tracking control decision should be de-
19 signed to force the disturbed system states to zero or a smaller neighborhood of the origin.

20 The sliding mode surface $s = s(x, t)$ (constructed by using the system states and corresponding
21 errors) defines the steady-state equivalent state. If the sliding variables s and \dot{s} can be driven to the
22 equivalent point within finite time in any initial condition, the actual system states approach the equiva-
23 lent point. In this way, the corresponding errors will converge to zero theoretically. To cope with
24 bounded disturbances/uncertainties and unknown perturbations, the following assumptions are made:

- 25 • A1. A sliding mode surface $s = s(x, t)$ exists, and the concerned system (2) can be driven to ap-
26 proach the desired equivalent state $s(x, t) = 0$.
- 27 • A2. The input-output dynamics of the considered system (2) can be transferred into a new system
28 that has a relative degree one with stable internal states [54,55].

29 Then, the dynamic (derivative) expression of the sliding variable s in the presence of unknown
30 perturbations is determined by

$$31 \quad \dot{s} = G(x) \left(\underbrace{\frac{\partial s}{\partial t} + \frac{\partial s}{\partial x} A(x) + \frac{\partial s}{\partial x} f(x, t)}_{\Xi(x, t)} + \underbrace{\frac{\partial s}{\partial x} B(x) \tilde{u}(t)}_{\Psi(x, t)} \right) = G(x) (\Xi(x, t) + \Psi(x, t) \tilde{u}(t)) \quad (3)$$

32 where $G(x)$ is a projection matrix to be designed later, $\tilde{u}(t)$ is the nominal control law, $\Xi(x, t)$
33 denote the complex perturbations. Along this line, the following assumptions are provided:

- 34 • A3. The complex uncertain function $\Xi(x, t)$ is rewritten using $\Xi(x, t) = \Xi_1(x, t) + \Xi_2(x, t)$,
35 where $|\Xi_1(x, t)| \leq \xi_1$, $|\Xi_2(x, t)| \leq \xi_2$ and $\xi_{i=1,2} > 0$ exist but are unknown.
- 36 • A4. The function $\Psi(x, t)$ can be determined by $\Psi(x, t) = \Psi_0(x, t) + \Delta\Psi(x, t)$ with $\Psi_0(x, t)$
37 being positive definite and $\Delta\Psi(x, t)$ being limited perturbation such that
38 $|\Delta\Psi(x, t)| / \Psi_0(x, t) \leq \Upsilon < 1$, $\forall x \in \square^n$ and $t \in [0, \infty)$, where Υ denotes an unknown boundary.

39 Consequently, we can reformulate (3) as

$$40 \quad \dot{s} = G(x) \left(\Xi(x, t) + \underbrace{\left(1 + \Delta\Psi(x, t) / \Psi_0(x, t) \right) \Psi_0(x, t)}_{\Psi_1(x, t)} \tilde{u}(t) \right) \quad (4)$$

$$41 \quad 1 - \Upsilon \leq \Psi_1(x, t) \leq 1 + \Upsilon \quad (5)$$

42 *A motivating example:* Under multiplicative time-varying perturbations (3), by utilizing the prior

1 knowledge of bounded perturbations (e.g., Lipschitz disturbances), *the traditional second order SMC*
 2 *mechanism can resolve the anti-disturbance control problem with guaranteed robustness.* By designing
 3 an appropriate controller, s and \dot{s} can approach the equivalent point within finite time. Given this
 4 context, the following conventional super-twisting-based SMC scheme [56,57] is described by

$$v(t) = -\eta_1 \square s^{\square^{1/2}} + \nu, \dot{\nu} = -\eta_2 \square s^{\square^0} \quad (6)$$

5 where η_1 and η_2 are the related control gains. This controller can drive s and its derivative \dot{s} to
 6 the equivalent point in finite time. Specifically, it offers a conventional second order SMC implementa-
 7 tion if $\eta_1 = 1.2\sqrt{M}$ and $\eta_2 = 1.1M$, where M denotes the upper boundary of the lumped perturba-
 8 tions. However, the adaptive gain regulation is not considered in this control scheme. In principle, one
 9 should use large control gains, but this may subtract unstable control responses [58]. The overestimated
 10 constant gains may lead to mitigated performance. Another concern is that the bounded information or
 11 the derivatives of the related lumped disturbances should be acquirable. This may be unavailable in the
 12 complex applications from the FMR system.

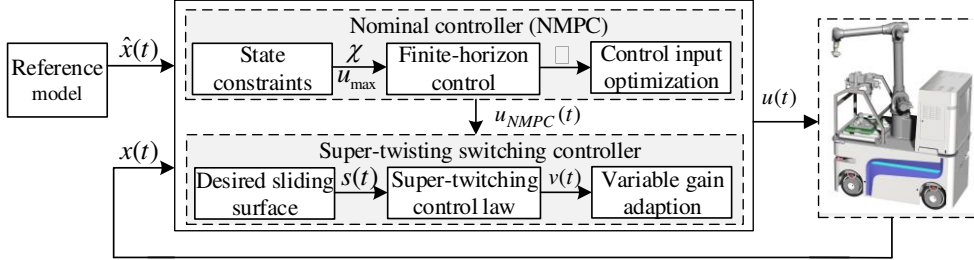
13 *Control objective:* Without requiring lumped disturbances boundary information (i.e., $\xi_{i=1,2}$ and
 14 Υ are unknown), a feasible control solution is desired to force s and \dot{s} to the equivalent point in
 15 finite time. To make the control gains applicable to multiplicative perturbations, an adap-
 16 tive-gain-scheduling rule is incorporated into the fractional super-twisting solution to handle the gain
 17 overestimation and chattering attenuation. Moreover, NMPC is explored to enhance the nominal lateral
 18 tracking performance of the FRM control system.

19 3. Main Results

20 To mitigate the design confusability, the hierarchical control framework is presented in Fig. 2. The
 21 NMPC method is used to generate the nominal control law $u_{NMPC}(t)$. The designed FRFTC can de-
 22 rive an anti-disturbance switching control action to make the states approach and remain on the desired
 23 sliding mode $s = 0$. Specifically, the optimized $u_{NMPC}(t)$ realizes the system control with the nomi-
 24 nal model as $\dot{x}(t) = A(x(t)) + B(x(t))u_{NMPC}(t)$. Then, the presented FRFTC scheme adopts the con-
 25 trol law calculated by the super-twisting method to mitigate the unknown perturbations. In this regard,
 26 the integrated control law is

$$u(t) = u_{NMPC}(t) + v(t) \quad (7)$$

27 Then, this optimized control mechanism can be achieved by the presented continuous-time NMPC
 28 method and additive anti-uncertainty/disturbance super-twisting switching regulation law, as indicated
 29 by the following results. For the concerned system, the uncertainty can be reduced.



30
 31 Fig. 2 Proposed FRFTC framework

32 3.1 Super-Twisting Switching Control Law

33 Inspired by the traditional super-twisting methods [45,46], the fractional-order variable gain
 34 switching control law is constructed as

$$v(t) = -\eta_1 \phi_1(s) - \eta_2 \phi_2(s) \quad (8)$$

$$\phi_1(s) = \tilde{\eta}_1 \square s^{\square^\alpha} + \tilde{\eta}_2 s \quad (9)$$

$$\dot{\phi}_2(s) = \dot{\phi}_1(s) \phi_1(s) = \tilde{\eta}_1^2 \alpha \square s^{\square^{2\alpha-1}} + (1 + \alpha) \tilde{\eta}_1 \tilde{\eta}_2 \square s^{\square^\alpha} + \tilde{\eta}_2^2 s \quad (10)$$

35 where $\tilde{\eta}_{i=1,2} \in \square^+$ denote the user-defined positive constants, $\alpha \in (0,1)$ denotes the specified frac-
 36 tional order, and $\eta_{i=1,2}(s, \dot{s}) \in \square^+$ denote the adaptive gains to be derived later.

37 Substituting (8) into (4) results in

$$\dot{s} = -\Psi_1(x) \eta_1 \phi_1(s) + \Xi_1(x) + Z \quad (11)$$

$$g_1(x)$$

$$\dot{Z} = -\Psi_1(x)\eta_2\phi_2(s) + \underbrace{\dot{\Xi}_2(x) + \eta_2\dot{\Psi}_1(x)\phi_2(s)}_{\dot{g}_2(x)} \quad (12)$$

1 Here, $\eta_2\dot{\Psi}_1(x)\phi_2(s)$ can be limited by an unknown factor ξ_3 , that is

$$|\eta_2\dot{\Psi}_1(x)\phi_2(s)| \leq |\eta_2\dot{\Psi}_1(x)| \int_0^t \dot{\phi}_2(s) d\tau \leq \xi_3 \quad (13)$$

2 The adaptive gain $\eta_2 = \eta_2(s, \dot{s})$ is bounded, that is $|\eta_2| \leq \eta_2^*$, where $\eta_2^* > 0$ denotes an uncer-
3 tain boundary. Then, one can obtain

$$|\eta_2\dot{\Psi}_1(x)\phi_2(s)| \leq \eta_2^*(1 + \Upsilon) \int_0^t (\tilde{n}_1^2 \alpha s^{2\alpha-1} + (1 + \alpha)\tilde{n}_1\tilde{n}_2 s^\alpha + \tilde{n}_2^2 s) d\tau \quad (14)$$

4 Then, the switching control problem is turned into seeking a control solution determined by (8)
5 -(10). In this way, s and \dot{s} can be driven to zero in finite time under unknown boundaries $\xi_{i=1,2,3}$,
6 $\Upsilon > 0$. The right hand of the control action (8) is a continuous function, whereas the additional inte-
7 grator (9) is discontinuous. Decreasing η_1 and η_2 is potential for reducing the chattering level.
8 However, this may increase the converge time.

9 **Theorem 1** Under the switching control law (8), a range of adaptive values exists such that the sliding
10 variables s and \dot{s} can be driven to the equivalent point within finite time if the following conditions
11 are satisfied:

12 i) with positive constants $\kappa, \delta, \mu, \varpi_{i=1,2}, \eta$ and η_m , the variable gains $\eta_{i=1,2}(s, \dot{s}, t)$
13 satisfy

$$\eta_1 \geq \delta + \frac{\{2\kappa(\xi_1 + 1) + \delta^2(2\xi_1 + 1) + 2\delta\xi_2 + \delta + \delta(\xi_1 + \xi_2)^2\}}{(2\kappa + 4\delta^2 - 2\delta)} \quad (15)$$

$$\dot{\eta}_1 = \begin{cases} \varpi_1 \sqrt{\omega_1/2} \text{sign}(|s| - \mu) & \text{if } \eta_1 > \eta_m \\ \eta & \text{if } \eta_1 \leq \eta_m \end{cases} \quad (16)$$

$$\eta_2 = (\kappa + 2\delta^2 + \delta\eta_1)/\delta \quad (17)$$

14 ii) a symmetric and positive definite matrix P and $\theta_{i=1,2} > 0$ can be selected such that

$$\begin{bmatrix} \tilde{A}^T P + P\tilde{A} + R & P\tilde{B} + \Omega^T \\ \tilde{B}^T P + \Omega & -\Theta \end{bmatrix} \leq 0 \quad (18)$$

15 where \tilde{A} and \tilde{B} are defined in (30), Θ and Ω are positive definite, and R is negative definite.

16 *Proof:* Theorem 1 is proven by providing analyses as below.

17 *Step 1.* The perturbation analysis over the switching phase

18 Denote a vector

$$\zeta^T = [\zeta_1, \zeta_2] = [\phi_1(s), Z] = [\tilde{n}_1 s^\alpha + \tilde{n}_2 s, Z] \quad (19)$$

19 Then, one can achieve

$$\dot{\zeta} = \dot{\phi}_1(s)[Z + g_1(x) - \eta_1\phi_1(s) \quad \dot{g}_2(x)/\phi_1(s) - \eta_2\phi_2(s)]^T = \dot{\phi}_1(s) \left(\begin{bmatrix} -\eta_1 & 1 \\ -\eta_2 & 0 \end{bmatrix} \zeta + \begin{bmatrix} 1 & 0 \\ 0 & 1 \end{bmatrix} \tilde{\rho} \right) \quad (20)$$

20 where $\tilde{\rho}(t, \zeta) = [g_1(x) \quad \dot{g}_2(x)|s|^{1-\alpha}/(\mu_1\alpha + \mu_2|s|^{1-\alpha})]^T$ and $\tilde{\rho}(t, \zeta)$ satisfy the sector conditions.

$$\begin{aligned} \omega_i(\tilde{\rho}_i, \zeta) &= [\tilde{\rho}_i(k, \zeta) - L_{i1}^T \zeta] [L_{i2}^T \zeta - \tilde{\rho}_i(k, \zeta)] \\ &= \begin{bmatrix} \tilde{\rho}_i \end{bmatrix}^T \begin{bmatrix} -1 & \star \\ 0.5(L_{i1}^T + L_{i2}^T) & -0.5(L_{i2}L_{i1}^T + L_{i1}L_{i2}^T) \end{bmatrix} \begin{bmatrix} \tilde{\rho}_i \\ \zeta \end{bmatrix}, \quad \forall L_{i1} \in \mathbb{R}^2, L_{i2} \in \mathbb{R}^2 \end{aligned} \quad (21)$$

21 where $i = 1, 2$.

22 According to (21), we have

$$\omega(\tilde{\rho}, \zeta) = \theta_1 \omega_1(\tilde{\rho}_1, \zeta) + \theta_2 \omega_2(\tilde{\rho}_2, \zeta) \geq 0, \quad \forall \theta_i \geq 0, i = 1, 2 \quad (22)$$

23 By using $\Theta = \begin{bmatrix} \theta_1 & 0 \\ 0 & \theta_2 \end{bmatrix}$, $R = -0.5 \sum_{i=1}^2 \theta_i (L_{i2}L_{i1}^T + L_{i1}L_{i2}^T)$, $\Omega = 0.5\Theta [L_{11}^T + L_{12}^T \quad L_{21}^T + L_{22}^T]^T$,

24 one can quadratically rewrite (22) as

$$\omega(\tilde{\rho}, \varsigma) = \begin{bmatrix} \tilde{\rho}(t, \varsigma) \\ \varsigma \end{bmatrix}^T \begin{bmatrix} -\Theta & \Omega \\ \Omega^T & R \end{bmatrix} \begin{bmatrix} \tilde{\rho}(t, \varsigma) \\ \varsigma \end{bmatrix} \geq 0 \quad (23)$$

1 Supposing that $L_{i2}^T = -L_{i1}^T = \tilde{g}_i [1 \ 0]$, $\tilde{g}_i > 0$, then we have $\omega_1(\tilde{\rho}_1, \varsigma) = -\tilde{\rho}_1(t, \varsigma) + \tilde{g}_1^2 \varsigma_1^2 \geq 0$
2 and $|\tilde{\rho}_1(k, \varsigma)| \leq \tilde{g}_1 |\varsigma_1|$. In original coordinates, this implies

$$|g_1(x)| \leq \tilde{g}_1 \left| \tilde{n}_1 |s|^{\alpha} + \tilde{n}_2 |s| \right| \leq \tilde{g}_1 \left(\tilde{n}_1 + \tilde{n}_2 |s|^{1-\alpha} \right) |s|^{\alpha} \quad (24)$$

3 Thus, one can conclude that $\xi_1 \geq \tilde{g}_1 \left(\tilde{n}_1 + \tilde{n}_2 |s|^{1-\alpha} \right)$ and $|\Xi_1(x, t)| = |g_1(t, x)| \leq \xi_1$. Moreover, the
4 graph $g_1(t, x)$ is limited by $\pm \tilde{g}_1 (\tilde{n}_1 |s|^{\alpha} + \tilde{n}_2 |s|)$. Moreover, owing to

$$\omega_2(\tilde{\rho}_2, \varsigma) = -\tilde{\rho}_2^2(t, \varsigma) + \tilde{g}_2^2 \varsigma_1^2 \geq 0 \quad (25)$$

5 $|\tilde{\rho}_2(t, \varsigma)| \leq \tilde{g}_2 |\varsigma_1|$ can be derived, that is

$$((\tilde{n}_1 \alpha)^{-1} |s|^{1-\alpha} + \tilde{n}_2^{-1}) |\dot{g}_2(x, t)| \leq \tilde{g}_2 \left| \tilde{n}_1 |s|^{\alpha} + \tilde{n}_2 |s| \right| \quad (26)$$

$$|\dot{g}_2(x, t)| \leq \tilde{g}_2 \left| \dot{\phi}_2(s) \right| = \tilde{g}_2 \left(\tilde{n}_1^2 \alpha / |s|^{1-2\alpha} + (1 + \alpha) \tilde{n}_1 \tilde{n}_2 |s|^{\alpha} + \tilde{n}_2^2 |s| \right) \quad (27)$$

6 This equation represents that nonlinearity $\dot{g}_2(x)$ is bounded by $\tilde{g}_2 / 2$. The above result pro-
7 vides a general analysis of the perturbations. For $\tilde{n}_1 = 0$, $\tilde{n}_2 = 1$, $L_{i2}^T = -L_{i1}^T = \tilde{g}_i [1 \ 0]$ and $\tilde{g}_i > 0$,
8 it is noted that $\omega_i(\tilde{\rho}_i, \varsigma) = \omega_i(\rho_i, x) = \tilde{g}_i^2 s^2 - \tilde{\rho}_i^2(t, x) \geq 0$ and $|\rho_i(t, x)| \leq \tilde{g}_i |s|$. Further, $\rho_i(k, x)$ is
9 limited by the lines $\tilde{g}_i s$ and $-\tilde{g}_i s$. In comparison, when $\tilde{n}_1 = 1$, $\tilde{n}_2 = 0$, $\varsigma^T = [|s|^{\alpha}, Z]$, we obtain

$$\tilde{\rho}(t, \varsigma) = \begin{bmatrix} \rho_1(t, s, Z) \\ |s|^{1-\alpha} \rho_2(t, s, Z) \\ \alpha \end{bmatrix} = \begin{bmatrix} \rho_1(t, |\phi_1(s)|^2, \varsigma_2) \\ |s|^{1-\alpha} \rho_2(t, |\phi_1(s)|^2, \varsigma_2) \\ \alpha \end{bmatrix} \quad (28)$$

10 For example, if $L_{i2}^T = -L_{i1}^T = \tilde{g}_i [1 \ 0]$, $\tilde{g}_i > 0$, then, $\omega_1(\tilde{\rho}_1, \varsigma) = \tilde{g}_1^2 s^2 - \tilde{\rho}_1^2(t, \varsigma) \geq 0$, that is
11 $|\tilde{\rho}_1(t, x)| \leq \tilde{g}_1 |\phi_1(s)|$. Thus, $g_1(t, x)$ is bounded within the sector $\tilde{g}_1 (|s|^{\alpha})$. Likewise,
12 $\omega_2(\tilde{\rho}_2, \varsigma) = \tilde{g}_2^2 s^2 - \tilde{\rho}_2^2(t, \varsigma) \geq 0$ is achieved, that is $|\tilde{\rho}_2(t, x)| \leq \tilde{g}_2 (|s|^{\alpha})$. In the original coordination,
13 $|\dot{g}_2(t, x)| \leq \tilde{g}_2 / 2$ implies that the boundary of $\dot{g}_2(t, x)$ is $\tilde{g}_2 / 2$.

14 *Step 2: Existence of control gains $\eta_{i=1,2}(s, \dot{s}, t)$*

15 Based on (11) and (12), a Lyapunov candidate is selected by using a quadratic form

$$V_1(s, z) = \varsigma^T P \varsigma \quad (29)$$

16 where $P = \begin{bmatrix} p_1 & p_3 \\ p_3 & p_2 \end{bmatrix}$ is a symmetric positive definite matrix.

17 Then, the following can be obtained

$$\dot{\varsigma} = \begin{bmatrix} \dot{\phi}_1(s) \{-\eta_1 \phi_1(s) + Z + g_1(x)\} \\ \dot{g}_2(x) - \eta_2 \dot{\phi}_1(s) \phi_1(s) \end{bmatrix} = \underbrace{\dot{\phi}_1(s) \begin{bmatrix} -\eta_1 & 1 \\ -\eta_2 & 0 \end{bmatrix} \begin{bmatrix} \phi_1(s) \\ Z \end{bmatrix}}_A + \underbrace{\dot{\phi}_1(s) \begin{bmatrix} 1 & 0 \\ 0 & 1 \end{bmatrix} \begin{bmatrix} g_1(x) \\ \dot{g}_2(x) \end{bmatrix}}_{\tilde{\rho}} \quad (30)$$

18 The consideration of $|D_1(x)| \leq \tilde{g}_1$ and $|D_2(x)| \leq \tilde{g}_2$ (with \tilde{g}_1, \tilde{g}_2 being the boundaries) leads to
19 $g_1(x) = D_1(x) \phi_1(s)$, $\dot{g}_2(x) = D_2(x) \dot{\phi}_2(s)$ (31)

19 Based on (31) and $\phi_2(s) = \dot{\phi}_1(s) \phi_1(s)$, one can achieve

$$\dot{\varsigma} = \underbrace{\dot{\phi}_1(s) \begin{bmatrix} -(\eta_1 - D_1(x)) & 1 \\ -(\eta_2 - D_2(x)) & 0 \end{bmatrix} \begin{bmatrix} \phi_1(s) \\ Z \end{bmatrix}}_A = \dot{\phi}_1(s) \Lambda \varsigma \quad (32)$$

20 Defining a symmetric matrix $Q = -\Lambda^T P - P \Lambda$ with a positive definite $P = \begin{bmatrix} \kappa + 2\delta^2 & -\delta \\ -\delta & \delta \end{bmatrix}$.

21 From (32), we have

$$Q = \begin{bmatrix} 2(\eta_1 - D_1)(\kappa + 2\delta^2) - 2\delta(\eta_2 - D_2) & \star \\ (\eta_2 - D_2)\delta - \delta(\eta_1 - D_1) - \kappa - 2\delta^2 & 2\delta \end{bmatrix} \quad (33)$$

1 By choosing $\eta_2 = \{\kappa + \delta^2 + \delta\eta_1\} / \delta$, one can achieve

$$Q - \begin{bmatrix} \delta & 0 \\ 0 & \delta \end{bmatrix} = \begin{bmatrix} 2\eta_1\kappa - 2D_1\kappa + 4\eta_1\delta^2 - 4D_1\delta^2 - 2\delta\eta_2 + 2\delta D_2 - \delta & \star \\ -\delta\eta_1 + \delta D_1 + \delta\eta_2 - \delta D_2 - \kappa - \delta^2 & \delta \end{bmatrix} \quad (34)$$

$$= \begin{bmatrix} \underbrace{\eta_1(2\kappa + 4\delta^2 - 2\delta) - 2\kappa(D_1 + 1) - 2\delta^2(2D_1 + 1) + 2\delta D_2 - \delta}_{E} & \star \\ \delta(D_1 - D_2) & \delta \end{bmatrix}$$

2 To achieve $Q - \text{diag}(\delta, \delta) \geq 0$, the full consideration of Algebraic Riccati Inequality results in

$$E - \delta(D_1 - D_2)\delta^{-1}\delta(D_1 - D_2) \geq 0 \quad (35)$$

3 Based on (15), Q is guaranteed to be positive definite satisfying $\lambda_{\min}(Q) \geq \delta$. Therefore, it is
4 concluded that

$$\dot{V}(s, Z) = \zeta^T P \zeta + \zeta^T P \dot{\zeta} = \dot{\phi}_1(s) \zeta^T (\Lambda^T P + P \Lambda) \zeta = -\dot{\phi}_1(s) \zeta^T Q \zeta \quad (36)$$

5 According to (30), the suitable positive constants $\theta_{i=1,2}$ can be chosen to fulfill the limitations of
6 the transformed perturbation. Thus, by selecting $L_{i2}^T = -L_{i1}^T = \tilde{g}_i [1 \ 0]$, the following Algebraic Ric-
7 cati Inequality is yielded

$$\tilde{A}^T P + P \tilde{A} + \delta P + R + (P \tilde{B} + \Omega^T) \Theta^{-1} (\tilde{B}^T P + \Omega) \geq \text{diag}\{\delta, \delta\} \quad (37)$$

8 or equivalently

$$\begin{bmatrix} \tilde{A}^T P + P \tilde{A} + R & P \tilde{B} + \Omega^T \\ \tilde{B}^T P + \Omega & -\Theta \end{bmatrix} \leq 0 \quad (38)$$

9 Further, the derivative of the candidate Lyapunov function $V_1(s, Z)$ can be calculated on the
10 same set $P^T = P$ as

$$\begin{aligned} \dot{V}_1 &= \dot{\phi}_1(s) \left\{ \zeta^T (\tilde{A}^T P + P \tilde{A}) \zeta + \tilde{\rho}^T \tilde{B} P \zeta + \zeta P \tilde{B} \tilde{\rho} \right\} \\ &= \dot{\phi}_1(s) \begin{bmatrix} \zeta \\ \tilde{\rho} \end{bmatrix}^T \begin{bmatrix} \tilde{A}^T P + P \tilde{A} & P \tilde{B} \\ \tilde{B}^T P & 0 \end{bmatrix} \begin{bmatrix} \zeta \\ \tilde{\rho} \end{bmatrix} \\ &\leq \dot{\phi}_1(s) \left\{ \begin{bmatrix} \zeta \\ \tilde{\rho} \end{bmatrix}^T \begin{bmatrix} \tilde{A}^T P + P \tilde{A} & P \tilde{B} \\ \tilde{B}^T P & 0 \end{bmatrix} \begin{bmatrix} \zeta \\ \tilde{\rho} \end{bmatrix} + \omega(\tilde{\rho}, \zeta) \right\} \\ &= \dot{\phi}_1(s) \begin{bmatrix} \zeta \\ \tilde{\rho} \end{bmatrix}^T \begin{bmatrix} \tilde{A}^T P + P \tilde{A} + R & P \tilde{B} + S^T \\ \tilde{B}^T P + S & -\Theta \end{bmatrix} \begin{bmatrix} \zeta \\ \tilde{\rho} \end{bmatrix} \end{aligned} \quad (39)$$

11 In view of (38), one can derive

$$\dot{V}_1 = -\dot{\phi}_1(s) \zeta^T Q(k, x) \zeta \leq -\varepsilon \dot{\phi}_1(s) \zeta^T \zeta \leq 0 \quad (40)$$

12 By using $\dot{\phi}_1(s) = (\alpha\mu_1 + \mu_2 |s|^{1-\alpha}) / |s|^{1-\alpha} \geq 0$, $\dot{V}_1(s, Z)$ is guaranteed to be negative definite.
13 Therefore, the closed-loop stability of the adaptive switching system can be guaranteed.

14 *Step 3: Finite time convergence analysis*

15 The following standard inequality is considered

$$\lambda_{\min}\{P\} \|\zeta\|_2^2 \leq \zeta^T P \zeta \leq \lambda_{\max}\{P\} \|\zeta\|_2^2 \quad (41)$$

16 where $\|\zeta\|_2^2 = \tilde{n}_1^2 |s|^{2\alpha} + 2\tilde{n}_1 \tilde{n}_2 |s|^{\alpha+1} + \tilde{n}_2^2 s^2 + Z^2$ denotes the Euclidean norm of ζ .

17 Then, $\mu_2 |s|^{1-\alpha} \leq \|\zeta\|_2 \leq \frac{V_1^{1/2}(s, Z)}{\lambda_{\min}^{1/2}\{P\}}$, $\|\zeta\|_2 \geq \frac{V_1^{1/2}(s, Z)}{\lambda_{\max}\{P\}}$, (40) can be expressed as

$$\begin{aligned}
\dot{V}_1 &\leq -\dot{\left((\alpha \tilde{n}_1 + \tilde{n}_2 |s|^{1-\alpha}) / |s|^{1-\alpha} \right)} \|\zeta\|_2^2 \\
&\leq -\dot{\left(\alpha \tilde{n}_1 \tilde{n}_2 / (\tilde{n}_2 |s|^{1-\alpha}) + \mu_2 \right)} \|\zeta\|_2^2 \\
&\leq -\frac{\alpha \tilde{n}_1 \tilde{n}_2 \lambda_{\min}\{P\}^{1/2}}{\underbrace{\lambda_{\max}\{P\}}_{\gamma_1(\tilde{n}_1)}} V_1^{1/2}(s, Z) - \frac{\tilde{\omega}_2}{\underbrace{\lambda_{\max}\{P\}}_{\gamma_2(\tilde{n}_2)}} V_1(s, Z)
\end{aligned} \tag{42}$$

1 The solution of

$$\dot{Y} = -\gamma_1(\tilde{n}_1)Y^{1/2} - \gamma_2(\tilde{n}_2)Y, Y(0) = Y_0 > 0 \tag{43}$$

2 can be derived as

$$Y(t) = \exp(-\gamma_2(\tilde{n}_2)t) \left[Y_0^{1/2} + \frac{\gamma_1(\tilde{n}_1)}{\gamma_2(\tilde{n}_2)} \left(1 - \exp\left(\frac{\gamma_2(\tilde{n}_2)}{2}t\right) \right) \right]^2 \tag{44}$$

3 Considering (42) and $V_1(t) \leq Y(t)$, s and \dot{s} converge to the origin in a finite time estimated by

$$T = \frac{2}{\gamma_2(\tilde{n}_2)} \ln \left(\frac{\gamma_2(\tilde{n}_2)}{\gamma_1(\tilde{n}_1)} V_1^{1/2}(s_0, Z_0) + 1 \right) \tag{45}$$

4 *Step 4:* Adaption of the control gains $\eta_{i=1,2}(s, \dot{s}, t)$

5 A Lyapunov candidate is constructed as

$$V(\zeta_{i=1,2}, \eta_1, \eta_2) = V_1 + (\eta_1 - \eta_1^*)^2 / (2\omega_1) + (\eta_2 - \eta_2^*)^2 / (2\omega_2) \tag{46}$$

6 where $\eta_1^* > 0$, $\eta_2^* > 0$ are positive constants.

7 Then, with $\dot{\omega}_\eta = \eta_1 - \eta_1^*$ and $\dot{\omega}_\eta = \eta_2 - \eta_2^*$, $r = \gamma_2(\tilde{n}_2) / \gamma_1(\tilde{n}_1)$, we obtain

$$\begin{aligned}
\dot{V}(\zeta_{i=1,2}, \eta_1, \eta_2) &= \zeta^T P \zeta + \dot{\omega}_\eta \dot{\eta}_1 / \omega_1 + \dot{\omega}_\eta \dot{\eta}_2 / \omega_2 \\
&\leq -r V_1^{1/2}(\zeta) + \dot{\omega}_\eta \dot{\eta}_1 / \omega_1 + \dot{\omega}_\eta \dot{\eta}_2 / \omega_2 \\
&= -r V_1^{1/2}(\zeta) - \varpi_1 |\dot{\omega}_\eta| / \sqrt{2\omega_1} - \varpi_2 |\dot{\omega}_\eta| / \sqrt{2\omega_2} + \dot{\omega}_\eta \dot{\eta}_1 / \omega_1 \\
&\quad + \dot{\omega}_\eta \dot{\eta}_2 / \omega_2 + \varpi_1 |\dot{\omega}_\eta| / \sqrt{2\omega_1} + \varpi_2 |\dot{\omega}_\eta| / \sqrt{2\omega_2}
\end{aligned} \tag{47}$$

8 With full consideration of $(x^2 + y^2 + z^2)^{1/2} \leq |x| + |y| + |z|$ and $\eta_0 \square \min(r, \varpi_1, \varpi_2)$, we have

$$-r V_1^{1/2}(\zeta) - \varpi_1 |\dot{\omega}_\eta| / \sqrt{2\omega_1} - \varpi_2 |\dot{\omega}_\eta| / \sqrt{2\omega_2} \leq -\eta_0 \sqrt{V(\zeta_{i=1,2}, \eta_1, \eta_2)} \tag{48}$$

9 From (48), (47) is rewritten as

$$\begin{aligned}
\dot{V}(\zeta_{i=1,2}, \eta_1, \eta_2) &\leq -\eta_0 \sqrt{V(\zeta_{i=1,2}, \eta_1, \eta_2)} + \dot{\omega}_\eta \dot{\eta}_1 / \omega_1 \\
&\quad + \dot{\omega}_\eta \dot{\eta}_2 / \omega_2 + \varpi_1 |\dot{\omega}_\eta| / \sqrt{2\omega_1} + \varpi_2 |\dot{\omega}_\eta| / \sqrt{2\omega_2}
\end{aligned} \tag{49}$$

10 Existing positive constants $\eta_1^* > 0$ and $\eta_2^* > 0$ satisfy $\eta_1 - \eta_1^* < 0$ and $\eta_2 - \eta_2^* < 0$, $\forall t > 0$.

11 Then, we can reformulate (49) as

$$\begin{aligned}
\dot{V}(\zeta_{i=1,2}, \eta_1, \eta_2) &\leq -\underbrace{\left| \dot{\omega}_\eta \left(\dot{\eta}_1 / \omega_1 - \varpi_1 / \sqrt{2\omega_1} \right) - \dot{\omega}_\eta \left(\dot{\eta}_2 / \omega_2 - \varpi_2 / \sqrt{2\omega_2} \right) \right|}_{\Gamma} \\
&\quad - \eta_0 \sqrt{V(\zeta_{i=1,2}, \eta_1, \eta_2)}
\end{aligned} \tag{50}$$

12 *Case 1:* For the case $|s| > \mu$ and $\eta_1 > \eta_m$ for $t > 0$. Then, in view of

$$\dot{\eta}_1 = \varpi_1 \sqrt{\omega_1 / 2}, \Gamma = -\left| \dot{\omega}_\eta \left(\dot{\eta}_2 / \omega_2 - \varpi_2 / \sqrt{2\omega_2} \right) \right| \tag{51}$$

13 if $\varpi_2 = \varpi_1$ and $\omega_2 = \omega_1$ are selected, the following can be obtained

$$\eta_2 = \kappa / \dot{\omega} + 2\dot{\omega} + \eta_1, \dot{\eta}_2 = \dot{\eta}_1 = \varpi_1 \sqrt{\omega_1 / 2}, \dot{\kappa} = \varpi_2 \sqrt{\omega_2 / 2} \tag{52}$$

14 The combination of (50) and (52) leads to

$$\dot{V}(\zeta_{i=1,2}, \eta_1, \eta_2) \leq -\eta_0 \sqrt{V(\zeta_{i=1,2}, \eta_1, \eta_2)} \tag{53}$$

15 As shown in Step 1, the control gain η_1 should meet the condition (15) to guarantee the finite

16 time convergence of the achieved system. Given this context, η_1 will increase based on (52) until (15)

is satisfied. This regulation ensures the positive definiteness of Q and the negative definiteness of $\dot{V}(\zeta_{i=1,2}, \eta_1, \eta_2)$. Thus, the finite time convergence is achieved in this case.

Case 2: For the case $|s| \leq \mu$,

$$\Gamma = \begin{cases} 2|\eta_1 - \eta_1^*| \varpi_1 / \sqrt{2\omega_1} & \text{if } \eta_1 > \eta_m \\ -|\eta_m - \eta_1^* + \eta t| \left(\eta / \omega_1 - \varpi_1 / \sqrt{2\omega_1} \right) & \text{if } \eta_1 \leq \eta_m \end{cases} \quad (54)$$

The control gain is defined by

$$\dot{\eta}_1 = \begin{cases} -\varpi_1 \sqrt{\omega_1 / 2} & \text{if } \eta_1 > \eta_m \\ \eta & \text{if } \eta_1 \leq \eta_m \end{cases} \quad (55)$$

It should be mentioned that the second term of (54) only holds in finite time as if $\eta_1 \leq \eta_m$. Moreover, η_1 will increase according to (55), that is $\dot{\eta}_1 = \eta_m + \eta \cdot t$. This ensures the positive definiteness of Γ . Hence, $|s|$ will increase, and as $|s| > \mu$, we will return to Case 1. Then, s reaches $|s| \leq \mu$ again in finite time, triggering the autonomous adaptive regulation of the control gains. In this manner, the convergence of the resultant system is guaranteed. This completes the proof.

Remark 2. Signum function (*sign*) is often used in the construction of the super-twisting switching control law to force the system to track the expected value [39]. However, near the sliding surface, the frequent switching of the signum function will cause undesirable chattering. Instead of the signum function, smooth functions such as saturation (*sat*)/hyperbolic tangent (*tanh*) can be used to alleviate the system oscillation [59]. This makes the discontinuous system in the traditional sliding mode into a smooth continuous switching system to suppress the chattering effectively.

Remark 3. The fractional super-twisting SMC algorithm guarantee that (15) is satisfied in finite time. Then, it can be concluded that s and \dot{s} are forced to the equilibrium domain $X = \{s, \dot{s} : |s| \leq J_1, |\dot{s}| \leq J_2, J_1 > \mu\}$ in finite time. $J_{i=1,2}$ is the control boundary. By using a straightforward integration of (50). The finite time can be estimated as $t_f = 2V^{1/2}(t_0) / \eta_0$.

3.2 NMPC-based Nominal Controller Design

In this subsection, a nominal NMPC control algorithm is designed to derive the continuous-time control law $u_{NMPC}(t)$. Under initial state $x(0) = x_0$ and uncertain perturbations $f(t)$, the finite-horizon NMPC scheme searches for a suitable nominal control input $\bar{u}_{[t_k, t_{k+N_c-1}|t_k]}$ by optimizing the criterion as below [60]

$$J \left(x, \bar{u}_{[t_k, t_{k+N_c-1}|t_k]}, N_c, N_p \right) = \int_{t_k}^{t_{k+N_p}} \left(|x(\tau)|_T^2 + |u(\tau)|_Q^2 \right) d\tau + V_f \left(x(t_{k+N_p}) \right) \quad (56)$$

$$\bar{u}_{[t_k, t_{k+N_c-1}|t_k]} = \left[u_0(t_k), u_1(t_k), \dots, u_{N_c-1}(t_k) \right] \quad (57)$$

$$|x(\tau)|_T^2 = x(\tau)^T T x(\tau), \quad |u(\tau)|_Q^2 = x(\tau)^T Q x(\tau) \quad (58)$$

under the following constraints

$$x(t) \in \mathcal{X}, x(t_{k+N_p}) \in \mathcal{X}_V, |u(t)| \leq u_{i_{\max}} - v_{i_{\max}}, t \in [t_k, t_{k+N_p}) \quad (59)$$

where t_k is the time instant, T and Q denote positive definite weight matrices, $N_c \geq 1$ and $N_p \geq N_c$ denote the control and prediction horizons, respectively, \mathcal{X} is the constraint sets of state,

$u_{i_{\max}}$ and $v_{i_{\max}}$ denote the limits of the control variables and the switching law, respectively,

$V_f(x) = |x|_W^2$ is the terminal penalty with W being a symmetric definite matrix, \mathcal{X}_V is the compact sets containing the origin as an interior point, which satisfies the following condition

$$\mathcal{X}_V = \left\{ x \mid |x|_W^2 \leq k_f \right\}, \mathcal{X}_V \subseteq \mathcal{X} \quad (60)$$

where k_f is a positive constant.

To derive the terminal penalty and set, design an auxiliary control law U_f as

$$U_f(e_i(t_k)) = K_g \left(\hat{x}(t_k) - x(t_k) \right) \quad (61)$$

1 where K_g is the control gain determined by infinite horizon linear quadratic control with the same
 2 cost function [61], and $\hat{x}(t_k)$ is the reference signal. Combining (59) and (60) results in

$$x(t_k) \in \mathcal{X}_V, \quad |U_f(e_i(t_k))| \leq u_{i_{\max}} - v_{i_{\max}}, \quad \forall x(t_{k-1}) \in \mathcal{X}_V \quad (62)$$

3 Therefore, $V_f(x)$ can be determined by

$$V_f(x(t_{k+1})) - V_f(x(t_k)) + \|x(t_k)\|_T^2 + \|U_f\|_Q^2 \leq 0 \quad (63)$$

4 where T , Q and W are the positive definite matrices of the algebraic Riccati equation

$$\|A(x(t_k)) - B(x(t_k))k_g\|_W^2 - W + Q + \|K_g\|_T^2 = 0 \quad (64)$$

5 By using the Receding Horizon strategy [62,63], the nominal NMPC optimized sequence
 6 $\bar{u}_{[t_k, t_{k+N_c-1}|t_k]}^{OP}$ is derived.

7 Then, the NMPC law in the interval $t \in [t_k, t_{k+1})$ can be obtained as

$$u_{NMPC}(t) = \bar{u}_{[t_k, t_{k+N_c-1}|t_k]}^{OP} \quad (65)$$

8 where $\bar{u}_{[t_k, t_{k+N_c-1}|t_k]}^{OP}$ is the first element of the optimized sequence at time instant t_k .

9 3.3 Anti-perturbation and Stability Aspects

10 **Theorem 2** For the concerned FMR system, the lumped disturbances (including the difference be-
 11 tween the dynamic nominal system and the evaluation of actual states) are compensated under the su-
 12 per-twisting SMC law.

13 *Proof:* As guaranteed by Theorem 1, the sliding surface variable and its derivative will approach
 14 zero in finite time and remain on it in the subsequent periods. By denoting $\partial s / \partial x = h(x)$ and
 15 $h(x) \neq 0$, (3) can be rewritten as

$$\dot{s} = G(x)h(x)(A(x) + f(x, t) + B(x)u_{NMPC}) \quad (66)$$

16 $g(x)$ is the desired reference trajectory without perturbations. By using an auxiliary variable

17 $s_a(u)$ as $s_a(u) = s(x) + g(x)$, the following can be obtained.

$$\dot{g}(x) = -G(x)h(x)(A(x) + B(x)u) \quad (67)$$

18 The consideration of $g(0) = 0$ yields

$$\dot{s}_a(u) = \dot{s}(x) + \dot{g}(x) = G(x)h(x)(A(x) + f(x, t) + B(x)u_{NMPC}) - G(x)h(x)(A(x) + B(x)u) \quad (68)$$

19 From (7) and $G(x) = h^{-1}(x)$, we have

$$v = B^{-1}(x)f(x, t) \quad (69)$$

20 From (69), one can conclude that the considered system operates in an undisturbed environment,
 21 then $u = u_{NMPC}$ can be obtained. This implies that the lumped disturbances/uncertainties can be well
 22 eliminated utilizing the designed super-twisting SMC law. This completes the proof.

23 **Theorem 3** Under the integrated control law (7), the global input-to-state practical stability of the
 24 concerned FMR system is ensured.

25 *Proof:* The recursive feasibility of the constraint state and the asymptotic stability of the system
 26 operation must be first proven.

27 Considering the optimal solution (65), the first element of $\bar{u}_{[t_k, t_{k+N_c-1}|t_k]}^{OP}$ is applied. During the
 28 recursion, consider the time instant t_{k+1} , and the first $N_c - 1$ sequence satisfies (59). At the time t_k ,
 29 the auxiliary variable satisfies the constraint conditions of (59) at any $j = N$, where j represents the
 30 sequence number. From (62), that $x(t_{k+N_c+1})$ satisfies (59) can be concluded. Thus, the stability proof
 31 of the system needs to consider the state continuity. Considering $t = t_k + \tau, \tau \in [0, T)$, the following
 32 variable is obtained

$$g_c(t) = [g_x(\tau, x(t_k), f_{[t_k, t]}) \quad g_u(\tau, x(t_k), 0)]^T \quad (70)$$

33 where $g_x(\tau, x(t_k), f_{[t_k, t]})$ is the state set at $t_{k+\tau}$, $g_u(\tau, x(t_k), 0)$ denotes the control sequence set at
 34 $t_{k+\tau}$ and $g_c(t)$ denotes the set of state and control law. We define the following Lyapunov candidate

$$V(t, g_c(t), N_c, N_p) = \int_0^{T-\tau} \left(|g_x(\zeta, x(t), 0)|_Q^2 + |g_u(\zeta, x_c(t), 0)|_R^2 \right) d\zeta \quad (71)$$

$$+ J \left(g(T-\tau, x(t_k), 0), \bar{u}_{[t_{k+1}, t_{k+N_c-1}|t_k]}^{OP}, N_c, N_p \right), t \in [t_k, t_{k+1})$$

1 where $\bar{u}_{[t_{k+1}, t_{k+N_c-1}|t_k]}^{OP}$ is the optimized control sequence at t_k .

2 Calculate the derivative of (71) as

$$\dot{V}(t, g_c(t), N_c, N_p) = \lim_{h \rightarrow 0^+} \left(\frac{V(t+h, g_c(t+h), N_c, N_p) - V(t, g_c(t), N_c, N_p)}{h} \right) \quad (72)$$

3 With (70), $g_c(t+h)$ is defined as

$$g_c(t+h) = [g_x(\tau+h, x(t_k), f_{[t_k, t+h]}) \quad g_u(\tau+h, x(t_k), 0)]^T \quad (73)$$

4 The numerator of (72) can be bounded as

$$\begin{aligned} & V(t+h, g_c(t+h), N_c, N_p) - V(t, g_c(t), N_c, N_p) \\ &= -\int_0^h \left(|g_x(\zeta, x(t), f)|_Q^2 + |g_u(\zeta, x(t), 0)|_R^2 \right) d\zeta + \int_0^{T-(\tau+h)} \left[|g_x(\zeta, x(t+h), f)|_Q^2 \right. \\ & \quad \left. - |g_x(\zeta, x(t+h|t), f)|_Q^2 + |g_u(\zeta, x(t+h), 0)|_R^2 - |g_u(\zeta, x(t+h|t), 0)|_R^2 \right] d\zeta \\ & \quad + \int_0^{(N_p-1)T} \left[|g(\zeta, x(t_{k+1}|t+h), u_{[t_{k+1}, t_{k+1+\zeta}|t_k]}^{OP}, f)|_Q^2 - |g(\zeta, x(t_{k+1}|t), u_{[t_{k+1}, t_{k+1+\zeta}|t_k]}^{OP}, f)|_Q^2 \right] \\ & \quad + \left(|u_{[t_{k+1}, t_{k+1+\zeta}|t_k]}^{OP}(t_{k+1}+\zeta)|_R^2 - |u_{[t_{k+1}, t_{k+1+\zeta}|t_k]}^{OP}(t_{k+1}+\zeta)|_R^2 \right) d\zeta + \\ & \quad V_f \left(g((N_p-1)T, x(t_{k+1}|t+h), u_{[t_{k+1}, t_{k+N_p}|t_k]}^{OP}, 0) \right) - V_f \left(g((N_p-1)T, x(t_{k+1}|t), u_{[t_{k+1}, t_{k+N_p}|t_k]}^{OP}, 0) \right) \end{aligned} \quad (74)$$

5 where $x(t_{k+1}|t)$ is the predicted state at time instant t , and $u_{[t_{k+1}, t_{k+1+\zeta}|t_k]}^{OP}(t_{k+1}+\zeta)$ is the control

6 sequence obtained at time $t_{k+1}+\zeta$. Under the constraints (59), when $t_k \in [kT, k(T+1)), \forall k$,

7 $u_{NMPC}(t)$ is a piecewise continuous constant. Auxiliary control can be reached via $U_f(t) = U_f(t+h)$,

8 $t+h \in [t_k, t_{k+1})$. $g((N_p-1)T, x(t_{k+1}|t+h), u_{[t_{k+1}, t_{k+N_p}|t_k]}^{OP}, 0)$ can be used to predict the dynamic

9 movement from the state $x(t_{k+1}|t+h)$ and obtain control law $u_{[t_{k+1}, t_{k+N_p}|t_k]}^{OP}$. In the prediction stage,

10 the new control law is obtained by using (56). Thus, the following is obtained

$$\lim_{h \rightarrow 0} x(t_{k+1}|t+h) = x(t_{k+1}|t), u(t) = u(t_k) \quad (75)$$

11 For $[t, t+h]$, G_a is determined basis on (74) and (75), i.e.,

$$G_a = \left(|g_x(\zeta, x(t), 0)|_Q^2 + |g_u(\zeta, x(t), 0)|_R^2 \right) \geq |g_x(\zeta, x(t), 0)|_Q^2 \geq \lambda_{\min}(Q) |g_x(\zeta, x(t), 0)|^2 \geq 0 \quad (76)$$

12 A straightforward calculation leads to

$$V(t+h, g_c(t+h), N_c, N_p) - V(t, g_c(t), N_c, N_p) \leq -hG_a \quad (77)$$

13 Substituting (77) into (72) yields

$$\dot{V}(t, x(t), N_c, N_p) \leq -G_a \quad (78)$$

14 Therefore, one can achieve

$$\dot{V}(t, g_c(t), N_c, N_p) \leq 0 \quad (79)$$

15 It should be noted that there may be a jump discontinuity of $V(t, g_c(t), N_c, N_p)$ at $t \in kT, \forall k$.

16 Then, it is necessary to prove the $V(t_k^+, g_c(t_k^+), N_c, N_p) \leq V(t_k^-, g_c(t_k^-), N_c, N_p)$, where t_k^+ and t_k^-

17 are the right and left limits of t_k , respectively. By defining $x(t_{k+1})$ and $x(t_{k+N_p}|t_{k+1})$, the follow-

1 ing can be stated

$$\begin{aligned}
V(t_{k+1}, g_c(t_{k+1}), N_c, N_p) &\leq J\left(x(t_{k+1}), u_{[t_k, t_{k+N_p}] | t_k}^{NP}, N_c, N_p\right) \\
&= V_f\left(g\left(NT, x(t_{k+1}), u_{[t_k, t_{k+N_p+1}] | t_{k+1}}^{NP}, 0\right)\right) - V_f\left(g\left(NT, x(t_k), u_{[t_k, t_{k+N_p}] | t_k}^{OP}, 0\right)\right) \\
&+ V\left(t_{k+1}^-, g\left(T^-, x(t_k), u_{[t_k, t_{k+1}] | t_k}^{OP}, f_{[t_k, t_{k+1}]}\right), N_c, N_p\right) \\
&- \int_0^T \left| g\left(\zeta, x(t_{k+N_p} | t_{k+1}), u_{[t_{k+N}, t_{k+N_c+1}] | t_{k+1}}^{NP}, 0\right) \right|^2 \\
&\leq V\left(t_{k+1}^-, g\left(T^-, x(t_k), u_{[t_k, t_{k+1}] | t_k}^{OP}, f_{[t_k, t_{k+1}]}\right), N_c, N_p\right)
\end{aligned} \tag{80}$$

2 Therefore, the following is derived

$$V(t_k^+, x(t_k^+), N_c, N_p) \leq V(t_k^-, x(t_k^-), N_c, N_p) \tag{81}$$

3 From (79) and (81) implies that $V(t, g_c(t), N_c, N_p)$ is decreasing. Therefore, the input-to-state
4 practical stability of the resultant FMR system can be guaranteed. This completes the proof.

5 4. Selection of the Control parameters

6 At this point, the selection of control parameters for specific implementation is analyzed:

7 1) In the practical application, a large fixed control gain is usually considered to ensure robust-
8 ness and anti-disturbance ability of the system if adaptive gain regulation is ignored, but this is usually
9 accompanied by a loss of dynamic tracking performance. Through (15), (16) and (17), an adaptive
10 regulation mechanism is proposed to improve the control flexibility. The specific criteria are as follows:

11 a) If $|s| > \mu$, $\eta_1 = \eta_1(0) + \varpi_1 \sqrt{\omega_1 / 2t}$ can be derived, where $\eta_1(0)$ is the related initial value and
12 $t \leq \tilde{t}$ with \tilde{t} is the finite reaching time; b) If $|s| \leq \mu$, η_1 and η_2 will decrease; c)

13 $\eta_2 = (\kappa + 2\delta^2 + \delta\eta_1) / \delta$ implies the same changing tendency of η_1 and η_2 . By adjusting the adaptive
14 step size η , $\varpi_1 \sqrt{\omega_1 / 2}$ and minimum gain η_m , the control method can make a trade-off between
15 disturbance suppression and control tracking performance. This scheme improves the anti-interference
16 ability of the system and avoids the system oscillation caused by overestimated gains.

17 2) According to the proposed controllers (9) and (10), the value range of fractional order α is
18 specified within (0.5, 1.5). The specific discussion is as follows: a) an integral control term when
19 $\alpha \in (1, 1.5)$; b) A derivative implementation when $\alpha \in (0.5, 1)$; c) An integer control term when $\alpha = 1$.
20 Fractional order parameters α can be selected flexibly. It is a feasible way to obtain the appropriate
21 fractional order by online adjustment, but the calculation will increase remarkably. Fortunately, the
22 characteristics of the FMR system determine that the value of the appropriate fractional order usually
23 varies within a small range. Meanwhile, an efficient optimization algorithm for obtaining the appro-
24 priate fractional order can greatly reduce the system workload. This ensures control efficiency and re-
25 duces the amount of calculation [64].

26 3) N_c and N_p represent the number of the parameters used to capture the future control trajectory
27 and the number of samples for predicting future state variables, respectively. Generally, a short N_c and
28 N_p will cause the oscillation of the closed-loop system. Especially in the underdamped system, large N_c
29 and N_p are required to achieve the expected performance. However, a larger range will bring a large
30 number of high-dimensional matrices, and the amount of calculation will increase substantially. Suita-
31 ble prediction and control horizons can greatly improve the tracking performance. It is noted that the
32 control horizon N_c should not be greater than the prediction horizon N_p [60]. In this paper, these related
33 parameters (i.e., N_c and N_p) are pre-tuned to enhance the tracking performance of the system.

34 5. Experimental Validation

35 5.1 Experimental Setup

36 Fig. 3 shows the self-developed FMR, and a real processing workshop is selected as the
37 experimental scenario. The FMR consists of a moving platform actuated by the in-wheel motors, a
38 manipulator equipped with an industrial camera to realize eye-in-hand vision-based operation, a storage
39 rack, LiDAR to measure the distance between the robot and unexpected obstacles to solving potential
40 collisions, and an IMU to obtain robotic acceleration and inclination. For a typical practical

1 implementation in a manufacturing factory, the operating environment may be very harsh. The severe
 2 environment includes damaged cover, oil/water, robot arm vibration, time-varying load, and other
 3 complex external interferences (as shown in Fig 3). This phenomenon is common in a traditional
 4 manufacturing factory, which will reduce friction and tire deformation. This may result in wheel slip
 5 and lateral swing. In addition, a large amount of lubricating oil and cooling water is required in the
 6 machining process of the machine tool. This inevitably leads to oil/water mixed ground conditions.
 7 Therefore, the factory ground conditions show uneven pavement, oil/water mixture and other complex
 8 road characteristics. The characteristics of unknown disturbance and uncertainty in an adaptive control
 9 environment lead to the change of controlled system parameters, structured or unstructured uncertainty
 10 and time-varying external disturbance. In the operation, the time-varying perturbations will lead to
 11 control instability (such as slipping and overturning) and other serious consequences. This may degrade
 12 achieving satisfactory system performance in terms of tracking accuracy and robustness. The specifica-
 13 tions of the developed platform are presented in Table 1.

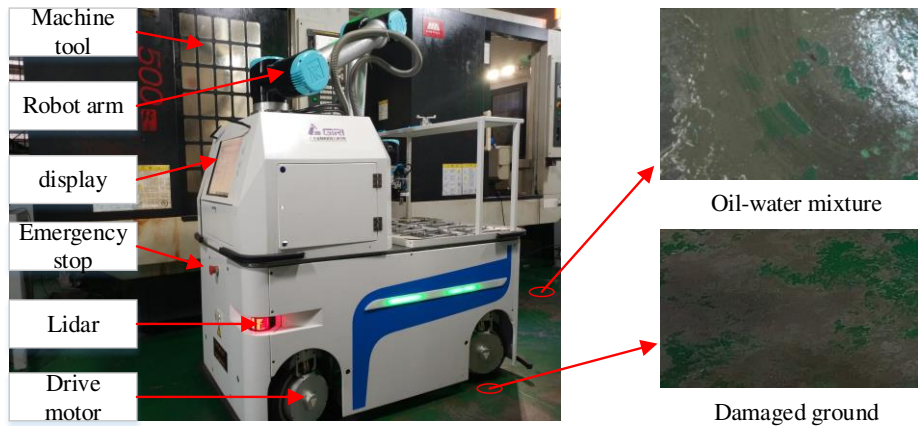


Fig. 3 Developed FMR and experiment scenario

Table 1 Specifications of the developed FMR system

Parameters	Values/Models	Parameters	Values/Models
Front wheelbase	0.48 m	Turning motor power	0.6 KW
Rear wheelbase	0.48 m	Driving motor power	11.35 KW
Robot width	0.56 m	Main frequency of PC	2.60 GHz
Robot mass	700 kg	LiDAR	HOKUYO UTM-30LX-EW
Yaw moment of inertia	130 kgm ²	Inertial measurement unit	LPMS-RS232AL2
Reduction ratio of tuning motor	60	Reduction ratio of driving motor	7.6

The developed FMR experimental platform is shown in Fig. 4, and the specific modules are described as follows:

1) Perception module: The real-time data can be acquired from external sensors such as LiDAR, IMU, ultrasonic, bumper, and infrared sensors. Therefore, the FMR system can realize the integration functions such as environmental understanding, object detection, and semantic place classification. Update the graph-based map information in real time to ensure the perception of the surrounding environment [65]. Then, a branch and bound algorithm-based global localization method is applied to sense the environment information by using the LIDAR [7]. Additionally, using scan matching and unscented distance filtering, an accurate and robust Monte Carlo localization-based pose tracking of FMR can be achieved to obtain a real-time robot pose [66]. Furthermore, an efficient re-localization solution is considered in the presence of environmental fluctuations to get the recovered robot pose with enhanced recovery speed and success rate. The current environment and state data collected in this module need to be transformed into a local coordinate system $X_R - O_R - Y_R$ that considers the FMR center as the origin and the length and width directions as the X and Y -axes. On the other hand, the center pixel point in the map is taken as the origin of the global coordinate system $X_G - O_G - Y_G$.

2) Decision-making module: The current lateral acceleration and driving torque of FMR can be obtained through an inertial measurement unit and servo driver. Therefore, the acquired data should be transformed by using the coordinate system [14]. It also carries out path-planning and navigation. To be more specific, a semantic topological map is applied to reduce the computational burden of global planning. Then, this module uses the industrial PC to make the control decision and sends them to the actuation module for motion decomposition through TCP/IP protocol. Its reasoning abilities exhibit more reasonable dynamic behaviors, and the decision-making module may derive an appropriate solution to handle the abnormal state of the FMR system to guarantee a safe operation.

3) Trajectory planning module: The multiple configurations of operating modes are incorporated into the construction of the desired profiles. Generally, the desired trajectories are generated by global

1 path planning while local planning is applied to resolve potential collisions. It is generalized to design a
 2 comprehensive optimized global path to reduce the calculation burden. As a common and effective
 3 strategy, a dynamic planning method is used to leverage the hybrid space of available modes with an
 4 incorporated exploration guiding algorithm. By utilizing the sampled sub goals and the constructed
 5 global path, local planning is then performed to avoid unexpected and potential obstacles. With
 6 state-space sampling, a near-time-optimal potential function local planning is realized to offer more
 7 comfortable clearance to both static and moving obstacles [2].

8 4) Direct yaw moment control module: The actuation and steering in arbitrary directions are realized
 9 by using the execution unit mainly includes a cooperative manipulator, dual-channel servo driver,
 10 in-wheel motors. The control and the execution layers use communication protocols to complete the
 11 information interaction. Specifically, communication between the control layer and the manipulator is
 12 realized by industrial Ethernet and interaction with motor adopts Ethernet bus. Moreover, the platform
 13 completes the omnidirectional movement by being equipped with eight servo motors, including 4
 14 steering motors and 4 hub motors. As a common and effective design strategy, the bus-type servo is
 15 used to realize the torque, current, and speed loop control method to the servo motor. By using the ob-
 16 tained environment information, position information, and reference trajectory, this module can calcu-
 17 late the executable control law and completely accurate, stable trajectory tracking.

18 This paper focuses on the controller design, and the specific process is shown in Fig. 2. By using the
 19 obtained environment information, position information, and reference trajectory, the direct yaw mo-
 20 ment controller can calculate the executable control law and perform accurate and stable trajectory
 21 tracking under the proposed DYMC framework.

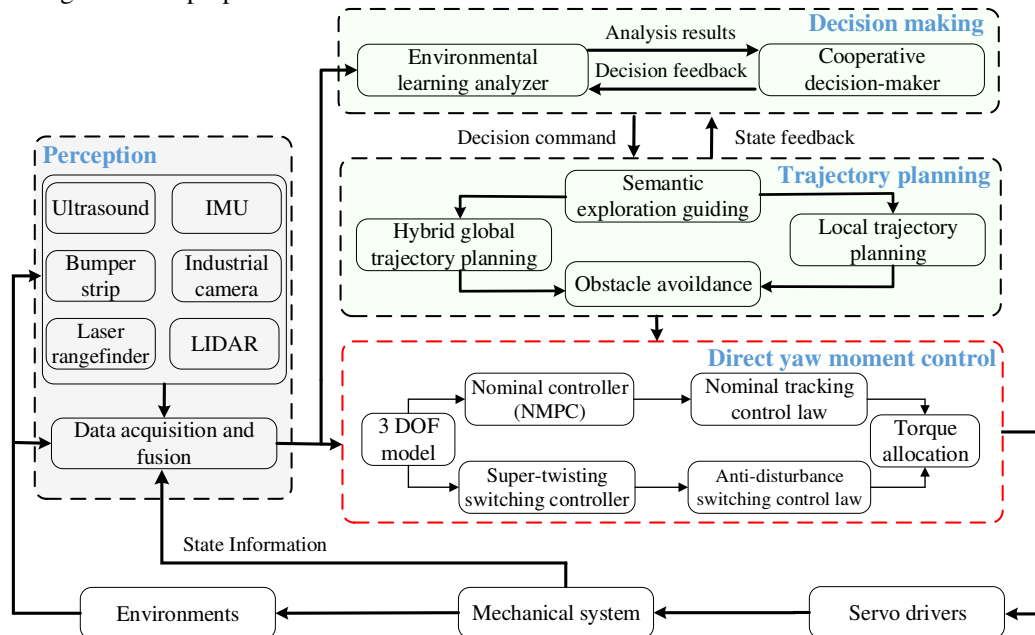


Fig. 4 Implementation framework of the developed FMR platform

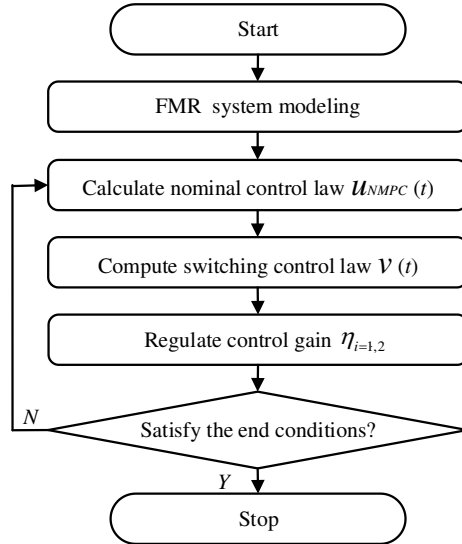


Fig. 5 Implementation of the proposed method

1
2
3
4
5
6
7
8
9
10
11
12
13

The specifications of the FMR and FRFTC are determined by $\tilde{n}_1 = \tilde{n}_2 = 1$, $\varpi_1 = 1.2$, $\omega_1 = 1.1$, $\dot{\delta} = 0.01$, $\beta = 1.1$, $\delta = 0.03$, $\mu = 0.012$, $\eta_m = 0.3$, $N_c = N_p = 10$ and $\alpha = 0.9$. As shown in Fig. 6, the FMR runs in Akerman mode by configuring the steering angles of the front wheel flexibly to adjust the steering radius. Experimental data are recorded and stored in real time on an industrial PC. The flow of control calculation, distribution and execution is as follows: the current data is processed in the data processing unit and returned to MATLAB. Then, the control algorithm can be implemented by using MATLAB. Finally, the control law is sent to the controller and servo to complete the whole closed-loop control process. All the controllers are tuned optimally with the same initial state of the considered robot, and the experiments are performed under the same operating conditions. To evaluate the presented FRFTC scheme, experiments are carried out according to Fig. 5 under different desired profiles and operating conditions as follows.

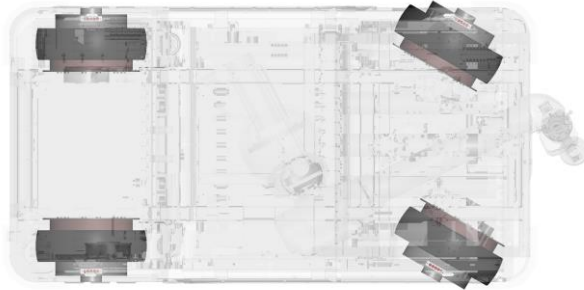


Fig. 6 Maneuvers models of the FMR

14
15
16
17
18
19
20
21
22
23
24
25
26
27
28
29
30
31
32
33

5.2 Experimental Results

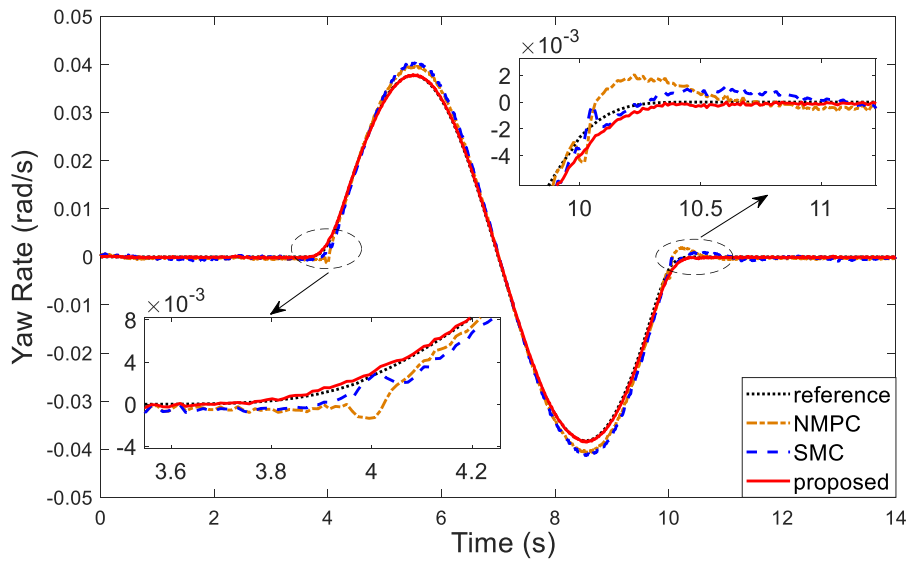
1) *Scenario 1*: This scenario is used to validate the tracking capacities under the proposed integrated method, the NMPC control method without the consideration of the anti-disturbance mechanism and the integer order SMC method. To ensure fairness, the parameter acquisition of NMPC and SMC is the same as that of the proposed method.

The yaw rate dynamic response and corresponding tracing errors are shown in Fig. 7 and Fig. 8, respectively. The comparison control schemes can guarantee that steady-state tracking in the resulting systems. As shown in these figures, our introduced integrated scheme can attain enhanced tracking responses compared with the traditional NMPC and SMC scheme. Specifically, the newly introduced method has the advantages of overshoot mitigation and tracking error reduction in terms of yaw rate tracking. On closer inspection, several distinct oscillations may be found in the transient tracking procedure by utilizing the conventional methods, whereas the resultant system using our proposed method can reduce the effects of lumped disturbances. Among these peaks, the maximum errors of NMPC, SMC and FRFTC methods are 0.00313, 0.0033 and 0.00054 *rad/s*, respectively, which show that the overshoot is reduced by 82.75 % and 83.64 % by employing our proposed FRFTC scheme. This finding implies that our proposed method can offer better tracking features with considerably mitigated dynamic tracing errors.

Fig. 9 to Fig. 12 show that the sideslip angle and speed tracking errors can be guaranteed to be

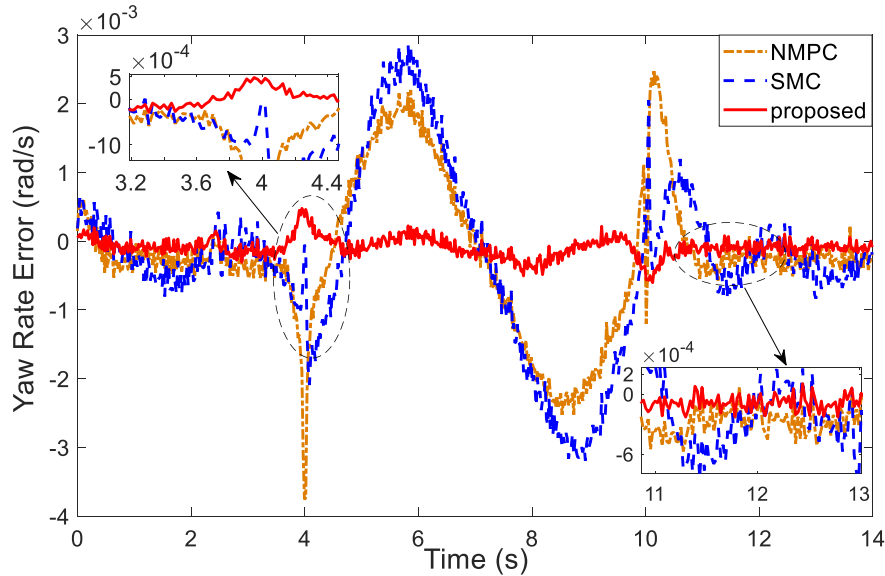
1 within a small range around the origin. Therefore, enhanced lateral tracking features can be verified.
 2 Some tracking vibrations can be observed with respect to the errors affected by the disturbances and
 3 uncertainties under the traditional NMPC and SMC method and the proposed anti-disturbance FRFTC
 4 method can diminish the effects of the perturbation, resulting in smaller tracking errors and steadier
 5 responses. Taking the sideslip angle for example, Fig. 11 shows that the overshoot amplitude under the
 6 NMPC and SMC method are 0.04383 and 0.0329 rad, respectively. The integrated method can achieve
 7 a smaller overshoot with a maximum error of 0.00471 rad. The overshoot amplitudes are reduced up to
 8 89.25 % and 85.68 %, respectively. This result ensures that the closed-loop system keeps the tracking
 9 trajectories close to the desired profiles, and the dynamic system is robust.

10 Fig. 13 and Fig. 14 depict the related control inputs, i.e., moment M_z and front steering angle
 11 δ_f , respectively. For the proposed adaptive finite time method, the vibration tendency of η_2 is
 12 shown in Fig. 15. As a benefit of its adaptive control gain regulation, the proposed method can offer
 13 smoother responses and improved stability for the considered FMR systems. By the obtained results in
 14 this scenario, the presented method can ensure the required control performance of the concerned FMR
 15 system compared with the conventional single NMPC and integer order SMC method under complex
 16 disturbed environments.



17
18

Fig. 7 Yaw rate tracking response in Scenario 1



19
20

Fig. 8 Yaw rate tracking errors in Scenario 1

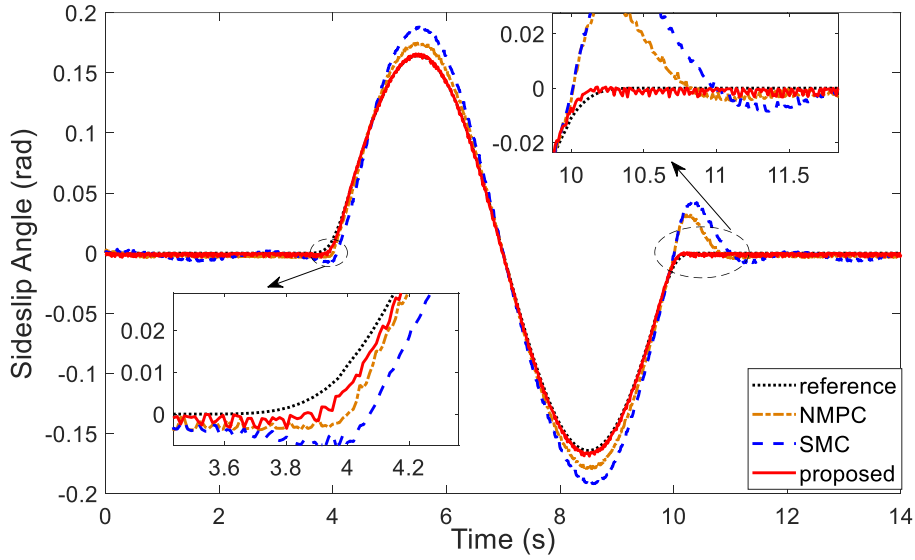


Fig. 9 Sideslip angle tracking responses in Scenario 1

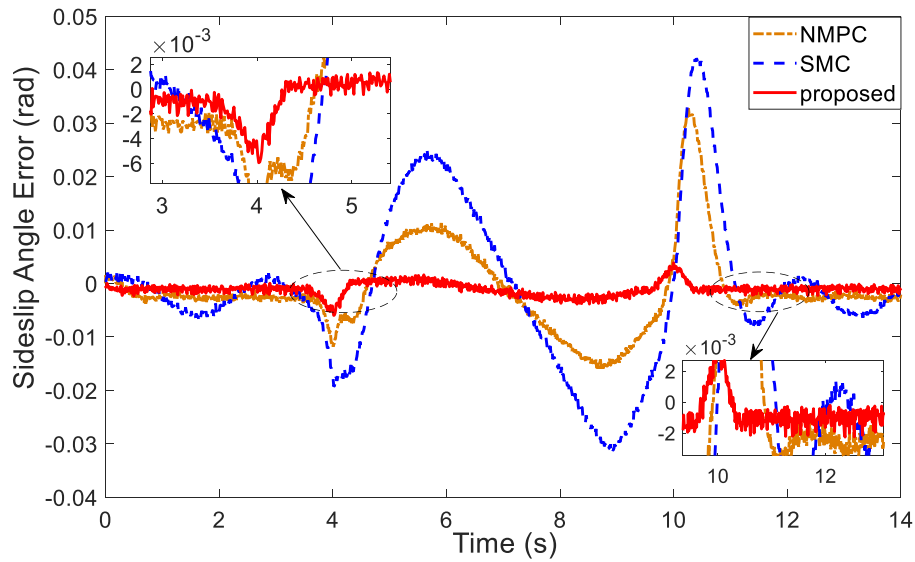


Fig. 10 Sideslip angle tracking errors in Scenario 1

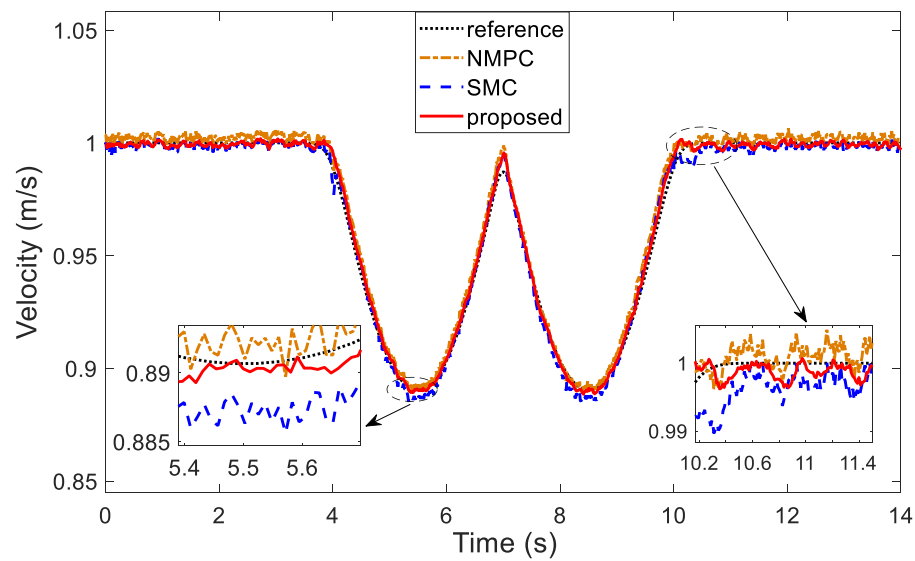


Fig. 11 Velocity tracking responses in Scenario 1

1
2

3
4

5
6

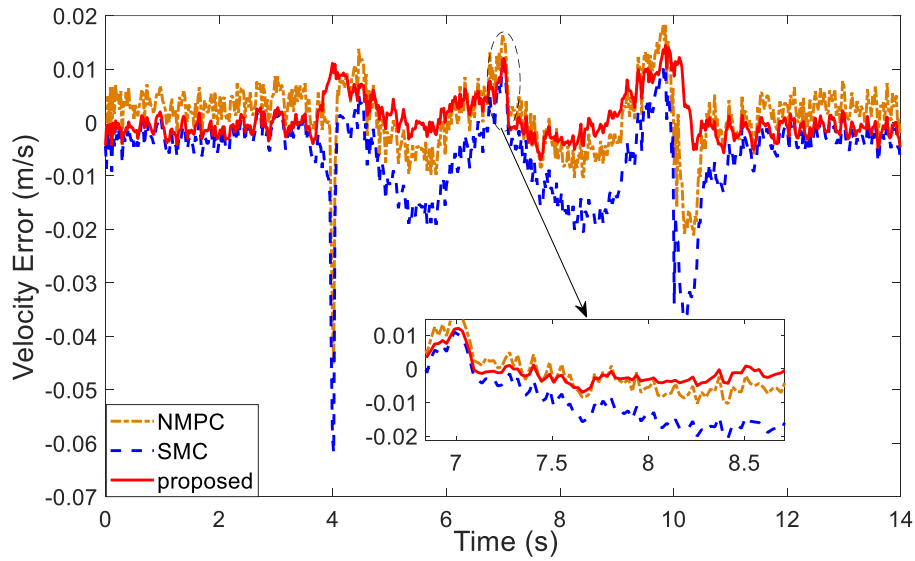


Fig. 12 Velocity tracking errors in Scenario 1

1
2

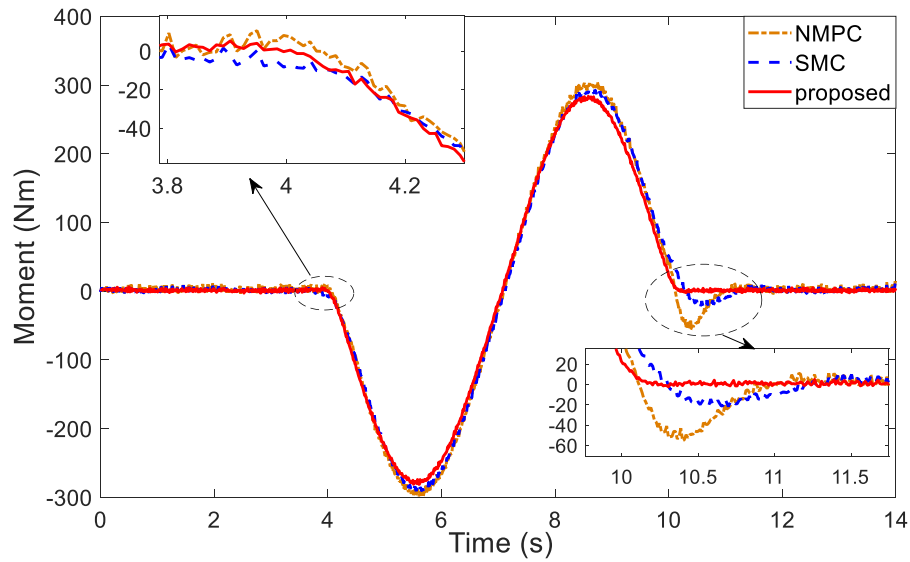


Fig. 13 Moment control inputs in Scenario 1

3
4

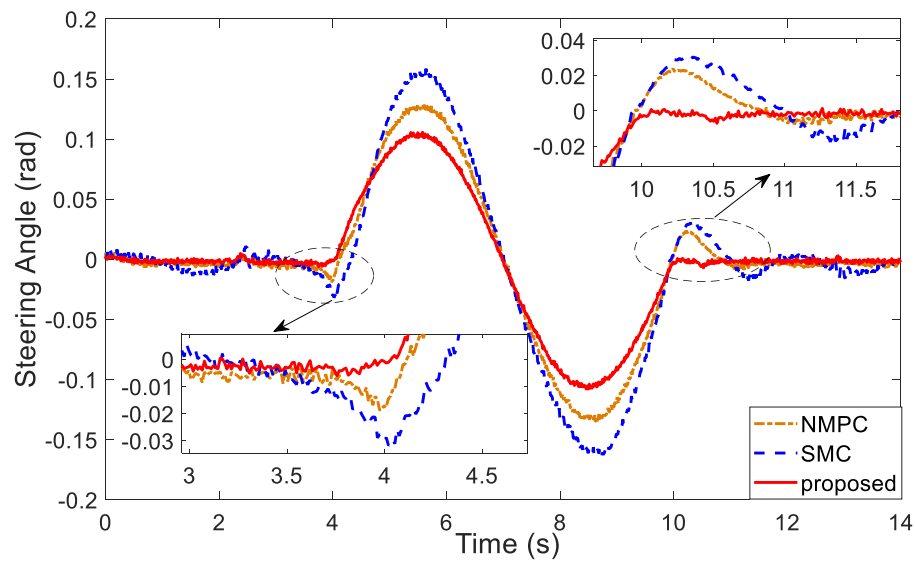


Fig. 14 Front steering angle in Scenario 1

5
6

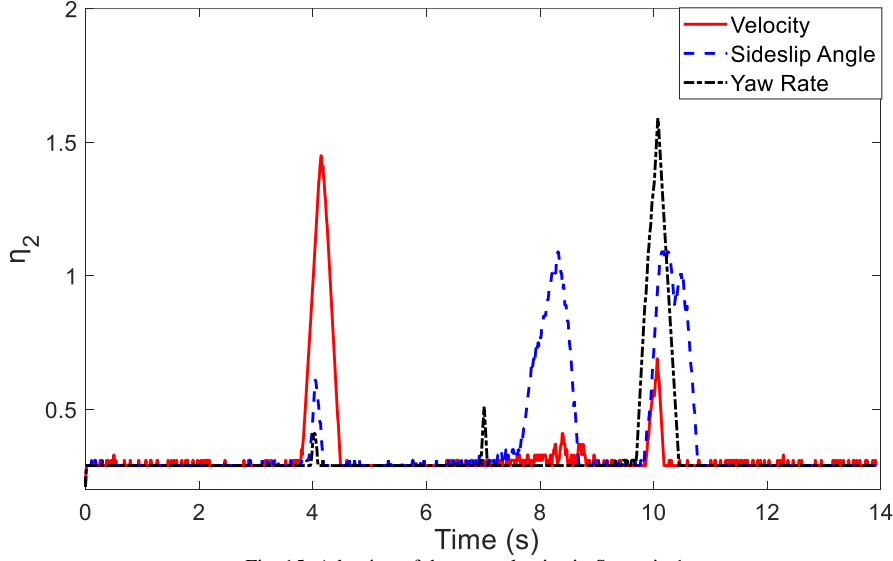


Fig. 15 Adaption of the control gains in Scenario 1

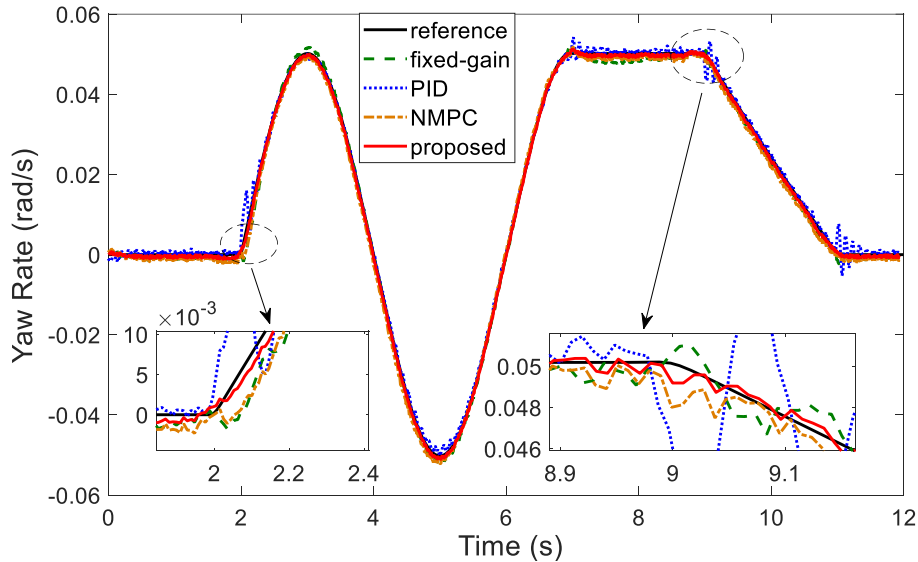
2) *Scenario 2*: To validate the adaptiveness and robustness of the presented FRFTC scheme, we evaluate the tracking control abilities in the slippery ground. The considered system may be disturbed by various disturbances such as unmodeled dynamics and payload variations as well as road surface conditions. In this scenario, the proportional-integral-derivative (PID) with optimally regulated parameters ($k_p = 1.2$, $k_i = k_d = 0.6$), the NMPC method without the consideration of the anti-disturbance mechanism and the proposed super-twisting FRFTC method with adaptive gains or fixed control gains for comparison are used. The natural-inspired optimization algorithm named artificial bee colony is used to acquire the stabilization control parameters of PID [67]. The fixed gain should consider tracking performance and interference suppression, and the gain is obtained (i.e., $\eta_2 = [0.36, 0.45, 0.23]$) by pre-tuning with a weight function.

Fig. 16 and Fig. 17 show the yaw rate results and the related following errors, respectively. As shown in Fig. 16, all comparison methods can achieve stable lateral tracing trajectories. Fig. 17 validates that the following system errors of the PID control scheme lead to larger vibrations, which mainly result from lumped disturbances and uncertainties. As a typical comparison, the presented adaptive control can obtain enhanced precision and smoother states. For instance, there exist overshoots with magnitudes of 0.00868, 0.0067, and 0.01034 *rad/s* under the fixed-gain, NMPC, and PID methods, respectively. The proposed adaptive scheme can mitigate these undesired overshoots, yielding a satisfactory yaw rate tracking performance during the whole control process. Similar results can be found in the sideslip angle tracking responses, as shown in Fig. 18 to Fig. 19. Fig. 20 and Fig. 21 depict the velocity tracking responses and related velocity errors, separately. Compared with our proposed method, the conventional PID, NMPC and the non-adaptive FRFTC schemes lead to non-ignorable overshoots. When subjected to unknown bounded perturbations, a great number of vibration changes with tremendous peaks in the traditional PID control systems are observed. Our presented adaptive FRFTC scheme provides more dynamical robustness to achieve resultant trajectories close to the reference ones. Specifically, the profiles of the tracking responses with respect to the sideslip angle are shown in Fig. 18 and Fig. 19, where a steady decrease is noted in the error peaks from over 0.04470 *rad* (with the PID method), 0.0127 *rad* (with the NSMC method) or 0.03866 *rad* (with the fixed-gain method) to approximately 0.00820 *rad* (with our proposed method).

Fig. 22 to Fig. 24 illustrate the related signals in terms of the yaw moment, steering angle, and the control gains using the comparison methods. Note that the adoption of variable gains is beneficial for efficaciously suppressing the lumped disturbances. Therefore, one can be applied to regulate the designed controller automatically to various operating conditions.

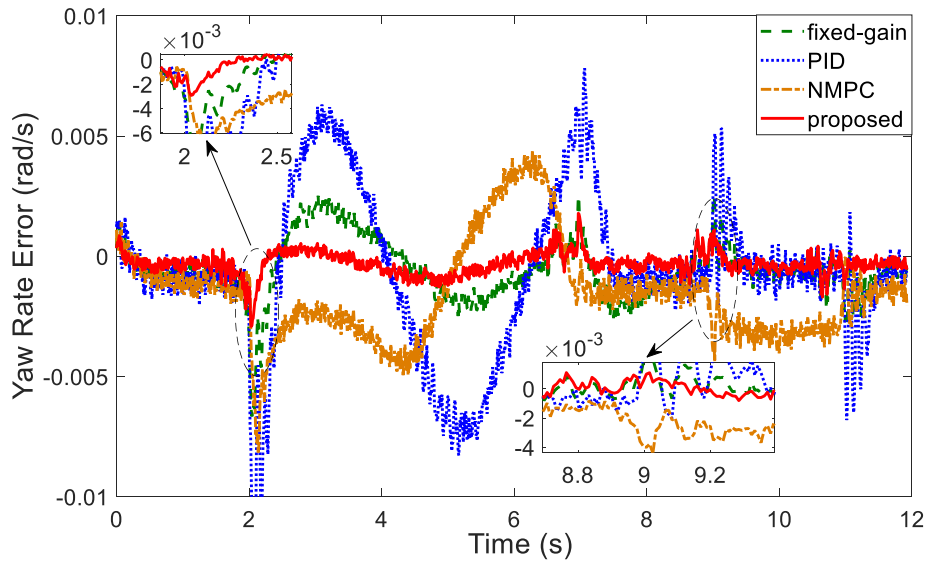
Overall, from the experimental results of *Scenario 1* and *Scenario 2*, it is obvious that the disturbance will degrade the performance of the controller system. Compared with other control methods, the proposed adaptive FTC law can achieve smoother response and smaller tracking errors with mitigated overshoots, thereby significantly improving the lateral motion control performance of the developed mobile robots. Specifically, the realization of the variable gain super-twisting SMC control scheme can make a trade-off between disturbance suppression and control tracking performance. In practice, the implementation process is simpler than other control methods because the upper boundary or correla-

1 tion derivatives of disturbance do not need to be considered. At the same time, the performance of the
 2 proposed integrated nonlinear robust adaptive controller is verified, which can effectively improve the
 3 handling stability of the mobile robot. Intuitively, it can be seen that the control input of the proposed
 4 control scheme is smoother than the traditional controller, which further improves the control perform-
 5 ance in the tracking process. Through the above analysis, a conclusion can be drawn that the designed
 6 coordination controller is feasible and effective in the process of path tracking. The proposed method
 7 can improve the tracking accuracy of mobile robots and improve the stability during operation.



8
9

Fig. 16 Yaw rate tracking response in Scenario 2



10
11

Fig. 17 Yaw rate tracking errors in Scenario 2

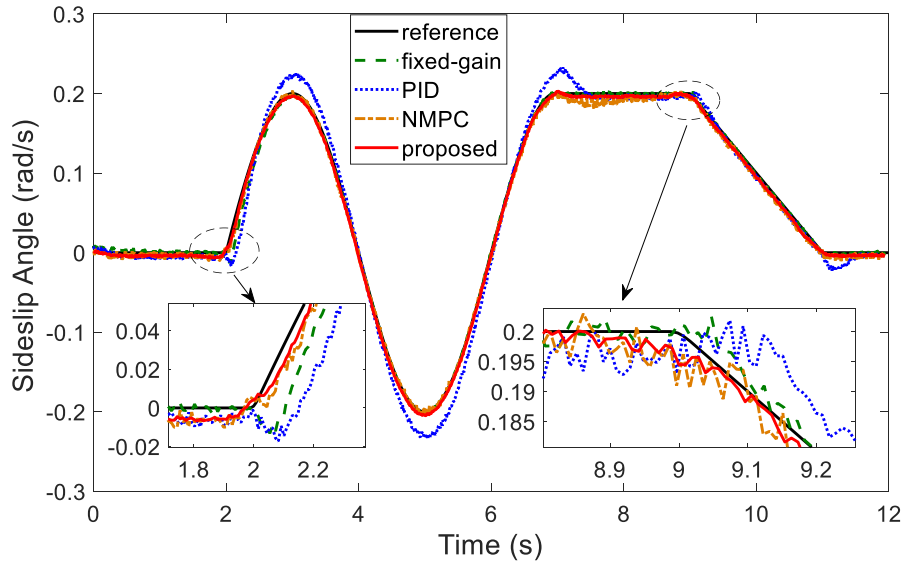


Fig. 18 Sideslip angle tracking responses in Scenario 2

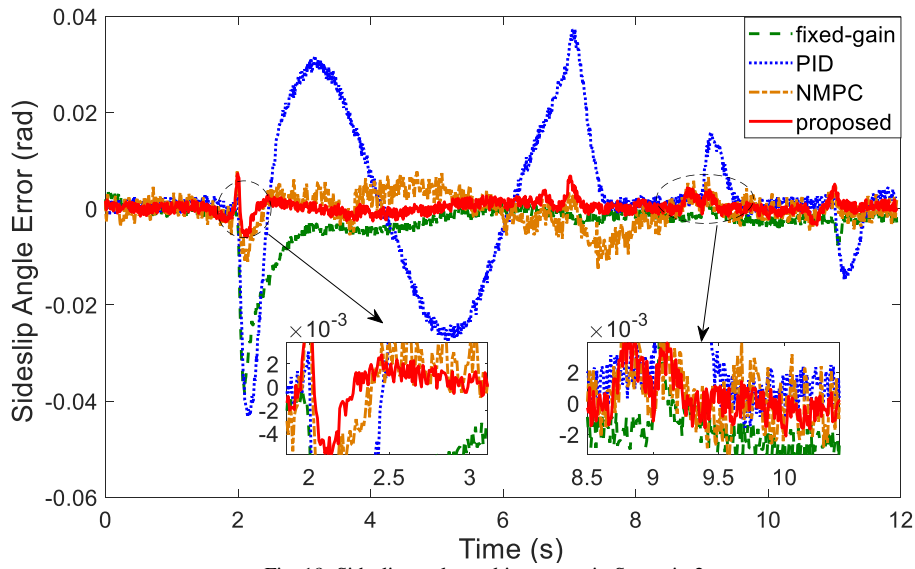


Fig. 19 Sideslip angle tracking errors in Scenario 2

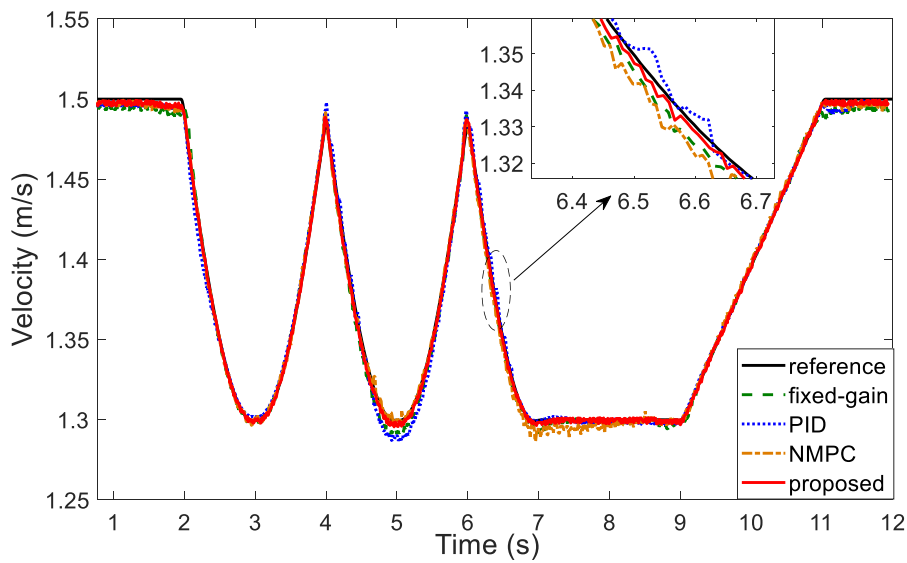


Fig. 20 Velocity tracking responses in Scenario 2

1
2

3
4

5
6

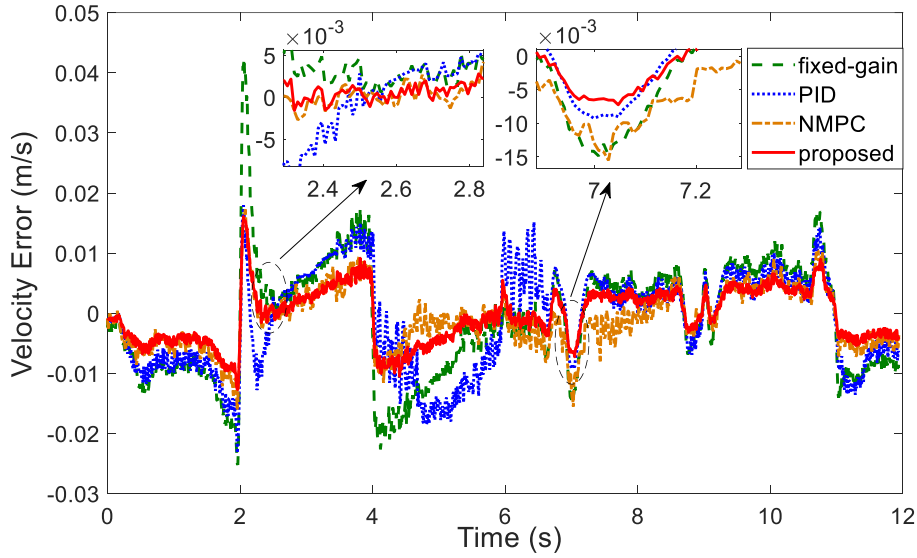


Fig. 21 Velocity tracking errors in Scenario 2

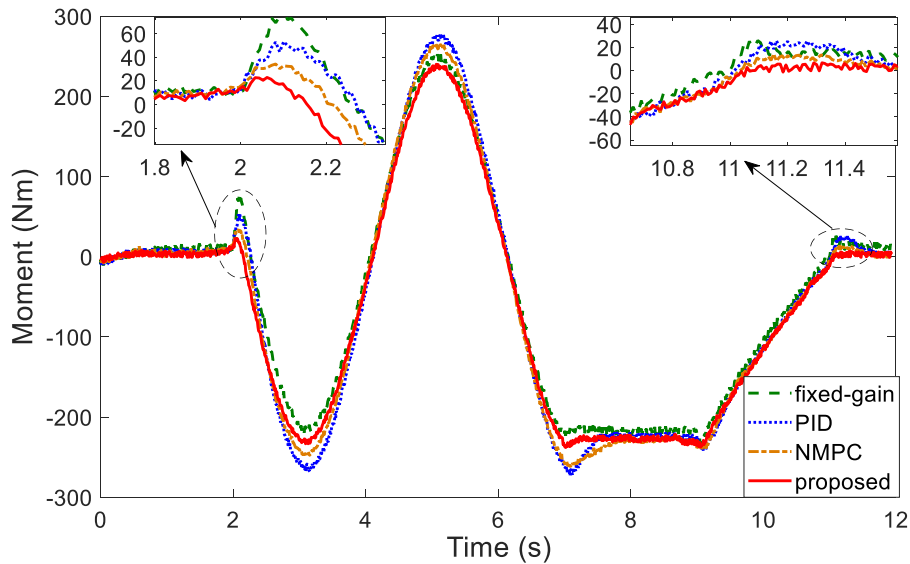


Fig. 22 Moment control inputs in Scenario 2

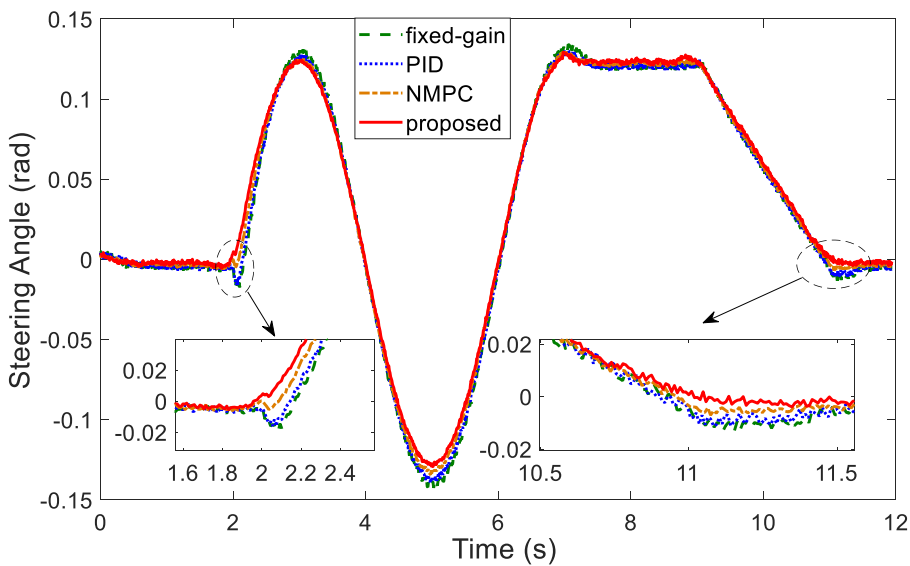


Fig. 23 Front steering angle in Scenario 2

1
2

3
4

5
6

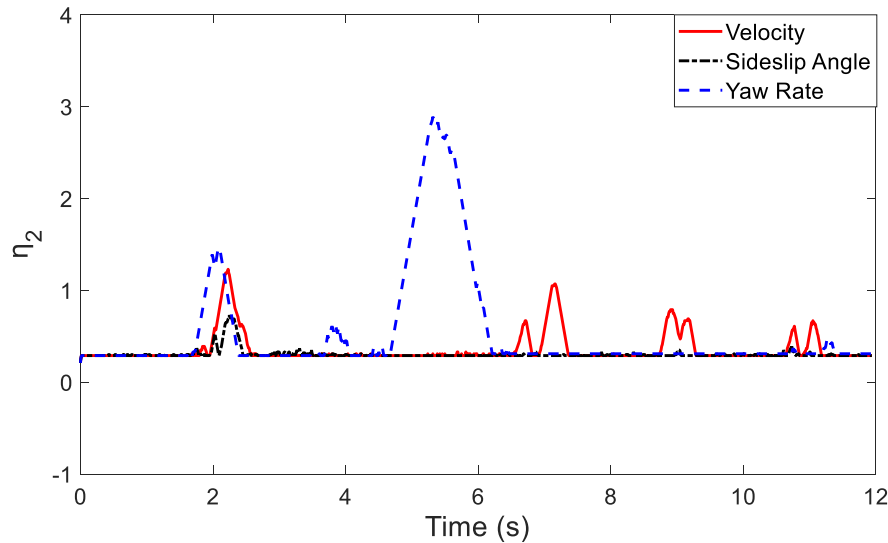


Fig. 24 Adaptation of the control gains in Scenario 2

6. Conclusions

An anti-disturbance adaptive FTC method is proposed to solve the robust stability of the nonlinear uncertain FMR system under the lateral motion control framework. Specifically, a novel fractional sliding-mode-based regulation is presented to force the states into a bounded region, which can be maintained for subsequent periods. The time-varying perturbations require the upper boundary or the related derivatives information by using the proposed method. Moreover, an enhanced piecewise continuous NMPC is integrated into the FRFTC framework to enhance the nominal tracing ability of the resulting FMR system. This control method can fulfill the state and input constraints and cancel out the unknown perturbations. Furthermore, the adaption of the variable gains is insensitive to the unknown disturbances and prevents the system from undesirable chattering caused by the high control gain. Moreover, the proposed method leads to a system that greatly alleviates the chattering phenomenon in the traditional SMC while guaranteeing system robustness. Theoretical analyses are conducted to prove the finite time convergence, anti-disturbance feature, and input-to-state practical stability of the achieved FMR system. Therefore, the proposed control scheme has the advantage of robust stabilization with the nonlinear uncertain FMR system under the lateral motion control framework. Finally, compared with the traditional control methods, the proposed control method can effectively alleviate the influence of centralized disturbance and uncertainty and can obtain high-precision lateral motion control. Thus, the feasibility and superiority of the FRFTC method are verified.

The anti-disturbance adaptive FRFTC of disturbed MIMO systems is investigated in this paper. However, for practical implementation, the hybrid time-varying delays might lead to system instability, especially for a high disturbing environment. Given this context, the robust control of time-delayed dynamical systems will be our future works to further enhance the closed-loop performance of the considered general FMR systems.

Acknowledgment

Funding: This work was supported by the National Natural Science Foundation of China under Grant No. 52105019; and the Guangdong Basic and Applied Basic Research Foundation under Grant No. 2020A1515110464 and No. 2021A1515012409.

References

- [1] Y. Chen, C. Stout, A. Joshi, M. L. Kuang, J. Wang, Driver-assistance lateral motion control for in-wheel-motor-driven electric ground vehicles subject to small torque variation, *IEEE Trans. Veh. Technol.* 67 (8) (2018) 6838-6850. <https://doi.org/10.1109/TVT.2018.2817514>.
- [2] Y. Xie, et al, Coupled fractional-order sliding mode control and obstacle avoidance of a four-wheeled steerable mobile robot, *ISA Trans.* 108 (2021) 282-294. <https://doi.org/10.1016/j.isatra.2020.08.025>.
- [3] H. Taheri, C. X. Zhao, Omnidirectional mobile robots, mechanisms and navigation approaches, *Mech. Mach. Theory* 153 (2020) 103958. <https://doi.org/10.1016/j.mechmachtheory.2020.103958>.
- [4] P. Kassaeyan, K. Alipour, B. Tarvirdizadeh, A full-state trajectory tracking controller for tractor-trailer wheeled mobile robots, *Mech. Mach. Theory* 150 (2020) 103872. <https://doi.org/10.1016/j.mechmachtheory.2020.103872>.
- [5] B. Liang, S. Zheng, C. K. Ahn, F. Liu, Adaptive fuzzy control for fractional-order interconnected systems with unknown control directions, *IEEE Trans. Fuzzy Syst.* (2020). <https://doi.org/10.1109/TFUZZ.2020.3031694>.
- [6] T. Terakawa, M. Komori, K. Matsuda, S. Mikami, A novel omnidirectional mobile robot with wheels connected by passive sliding joints, *IEEE/ASME Trans. Mechatron.* 23 (3) (2017) 1716-1727. <https://doi.org/10.1109/TMECH.2019.2892489>.
- [7] J. Meng et al., Iterative-learning error compensation for autonomous parking of mobile manipulator in harsh industrial environment, *Robot. Comput. Integr. Manuf.* 68 (2021) 102077. <https://doi.org/10.1016/j.rcim.2020.102077>.

- 1 [8] H. Jiang, G. Xu, W. Zeng, G. Feng, Design and kinematic modeling of a passively-actively transformable mobile robot,
2 Mech. Mach. Theory 142 (2019) 103591. <https://doi.org/10.1016/j.mechmachtheory.2019.103591>.
- 3 [9] J. Guo, Y. Luo, K. Li, Y. Dai, Coordinated path-following and direct yaw-moment control of autonomous electric vehicles
4 with sideslip angle estimation, Mechanical Syst. Signal Proce. 105 (2018) 183-199.
5 <https://doi.org/10.1016/j.ymssp.2017.12.018>.
- 6 [10] X. Wu, Y. Huang, Adaptive fractional-order non-singular terminal sliding mode control based on fuzzy wavelet neural
7 networks for omnidirectional mobile robot manipulator, ISA Trans. (2021). <https://doi.org/10.1016/j.isatra.2021.03.035>
- 8 [11] Y. Xie, X. Tang, S. Zheng, W. Qiao, S. Song, Adaptive fractional order PI controller design for a flexible swing arm system
9 via enhanced virtual reference feedback tuning, Asian J. Control, 20 (3) (2018) 1221-1240.
10 <https://doi.org/10.1002/asjc.1633>.
- 11 [12] S. Kaur, S. Narayan, Fractional order uncertainty estimator based hierarchical sliding mode design for a class of fractional
12 order non-holonomic chained system, ISA Trans. 77(2018) 77: 58-70. <https://doi.org/10.1016/j.isatra.2018.04.004>
- 13 [13] A. J. Muñoz-Vázquez, F. Gaxiola, F. Martínez-Reyes, A. AlainManzo-Martínez, A fuzzy fractional-order control of robotic
14 manipulators with PID error manifolds, Appl. Soft Comput. 83 (2019) 105646. <https://doi.org/10.1016/j.asoc.2019.105646>
- 15 [14] J. Meng, et al., Robust Lateral Stabilization Control of In-Wheel-Motor-Driven Mobile Robots via Active Disturbance
16 Suppression Approach, Sensors 20 (18) (2020) 5238. <https://doi.org/10.3390/s20185238>.
- 17 [15] K. Alipour, A. B. Robat, B. Tarvirdizadeh, Dynamics modeling and sliding mode control of tractor-trailer wheeled mobile
18 robots subject to wheels slip, Mech. Mach. Theory 138 (2019) 16-37.
19 <https://doi.org/10.1016/j.mechmachtheory.2019.03.038>.
- 20 [16] P. Kassaeiyan, B. Tarvirdizadeh, K. Alipour, Control of tractor-trailer wheeled robots considering self-collision effect and
21 actuator saturation limitations, Mechanical Syst. Signal Proce. 127 (2019) 388-411.
22 <https://doi.org/10.1016/j.ymssp.2019.03.016>.
- 23 [17] J. Liao, Z. Chen, B. Yao, Model-based coordinated control of four-wheel independently driven skid steer mobile robot with
24 wheel-ground interaction and wheel dynamics, IEEE Trans. Ind. Inf. 15(3) (2018) 1742-1752.
25 <https://doi.org/10.1109/TII.2018.2869573>.
- 26 [18] M. Duan, J. Jia, T. Ito, Fast terminal sliding mode control based on speed and disturbance estimation for an active suspen-
27 sion gravity compensation system, Mech. Mach. Theory 155 (2021) 104073.
28 <https://doi.org/10.1016/j.mechmachtheory.2020.104073>.
- 29 [19] H. Y. Chen, et al, Development of a novel leg-wheel module with fast transformation and leaping capability, Mech. Mach.
30 Theory 163 (2021) 104348. <https://doi.org/10.1016/j.mechmachtheory.2021.104348>.
- 31 [20] Y. Chen, Z. Li, H. Kong, F. Ke, Model predictive tracking control of nonholonomic mobile robots with coupled input con-
32 straints and unknown dynamics, IEEE Trans. Ind. Inf. 15 (6) (2018) 3196-3205. <https://doi.org/10.1109/TII.2018.2874182>.
- 33 [21] J. Liu, Z. Wang, L. Zhang, P. Walker, Sideslip angle estimation of ground vehicles: a comparative study, IET Control The-
34 ory Appl. 14 (20) (2020) 3490-3505. <https://doi.org/10.1049/iet-cta.2020.0516>.
- 35 [22] A. K. Khalaji, M. Jalalnejhad, Robust forward/backward control of wheeled mobile robots, ISA Trans. (2021).
36 <https://doi.org/10.1016/j.isatra.2021.01.016>.
- 37 [23] J. Zhang, S. Zhou, F. Li, J. Zhao, Integrated nonlinear robust adaptive control for active front steering and direct yaw mo-
38 ment control systems with uncertainty observer, Trans. Inst. Meas. Control 42(16) (2020) 3267-3280.
39 <https://doi.org/10.1177/0142331220949718>.
- 40 [24] S. Ding, L. Liu, W. X. Zheng, Sliding mode direct yaw-moment control design for in-wheel electric vehicles, IEEE Trans.
41 Ind. Electron. 64 (8) (2017) 6752-6762. <https://doi.org/10.1109/TIE.2017.2682024>.
- 42 [25] A. L. Lindqvist, S. Zhou, P. D. Walker, Direct yaw moment control of an ultra-lightweight solar-electric passenger vehicle
43 with variation in loading conditions, Vehicle Syst. Dyn. (2020) 1-23. <https://doi.org/10.1080/00423114.2020.1853784>.
- 44 [26] N. Ahmadian, A. Khosravi, P. Sarhadi, Integrated model reference adaptive control to coordinate active front steering and
45 direct yaw moment control, ISA Trans. 106 (2020) 85-96. <https://doi.org/10.1016/j.isatra.2020.06.020>.
- 46 [27] B. Lenzo, M. Zanchetta, A. Sorniotti, P. Gruber, Yaw rate and sideslip angle control through single input single output
47 direct yaw moment control, IEEE Trans. Control Syst. Technol. 29 (1) (2021) 124-139.
48 <https://doi.org/10.1109/TCST.2019.2949539>.
- 49 [28] D. Wu, Y. Cheng, H. Du, W. Zhu, M. Zhu, Finite-time output feedback tracking control for a nonholonomic wheeled mo-
50 bile robot, Aeros. Sci. Technol. 78 (2018) 574-579. <https://doi.org/10.1016/j.ast.2018.05.005>.
- 51 [29] J. Zhai, Z. Song, Adaptive sliding mode trajectory tracking control for wheeled mobile robots, Int. J. Control 92(10) (2019)
52 2255-2262. <https://doi.org/10.1080/00207179.2018.1436194>.
- 53 [30] C. Lian, X. Xu, H. Chen, H. He, Near-Optimal Tracking Control of Mobile Robots Via Receding-Horizon Dual Heuristic
54 Programming, IEEE Trans. Cybern. 46(11) (2016) 2484-2496. <https://doi.org/10.1109/TCYB.2015.2478857>.
- 55 [31] C. Hwang, H. Wu, W. Hung, Software/Hardware-Based Hierarchical Finite-Time Sliding-Mode Control With Input Satur-
56 ation for an Omnidirectional Autonomous Mobile Robot, IEEE Access 7 (2019) 90254-90267.
57 <https://doi.org/10.1109/ACCESS.2019.2926514>.
- 58 [32] X. Zhang, R. Wang, Y. Fang, B. Li, B. Ma, Acceleration-Level Pseudo-Dynamic Visual Servoing of Mobile Robots With
59 Backstepping and Dynamic Surface Control, IEEE Trans. Syst., Man, Cybern.: Syst. 49(10) (2019) 2071-2081.
60 <https://doi.org/10.1109/TSMC.2017.2777897>.
- 61 [33] Y. Wang, Z. Wang, L. Zhang, M. Liu, J. Zhu, Lateral stability enhancement based on a novel sliding mode prediction con-
62 trol for a four-wheel-independently actuated electric vehicle, IET Intell. Trans. Syst. 13(1) (2019) 124-133.
63 <https://doi.org/10.1049/iet-its.2017.0407>.
- 64 [34] Z. Sun, H. Xie H, J. Zheng, Z. Man, D. He, Path-following control of Mecanum-wheels omnidirectional mobile robots
65 using nonsingular terminal sliding mode, Mechanical Syst. Signal Proce. 147 (2021) 107128.
66 <https://doi.org/10.1016/j.ymssp.2020.107128>.
- 67 [35] L. Zhang, Y. Wang, Z. Wang, Robust lateral motion control for in-wheel-motor-drive electric vehicles with network in-
68 duced delays, IEEE Trans. Veh. Technol. 68(11) (2019) 10585-10593. <https://doi.org/10.1109/TVT.2019.2942628>.
- 69 [36] J. Li, J. Wang, H. Peng, Y. Hu, H. Su, Fuzzy-torque approximation-enhanced sliding mode control for lateral stability of
70 mobile robot, IEEE Trans. Syst., Man, Cybern.: Syst. (2021). <https://doi.org/10.1109/TSMC.2021.3050616>.
- 71 [37] S. Lee, D. Chwa, Dynamic Image-Based Visual Servoing of Monocular Camera Mounted Omnidirectional Mobile Robots
72 Considering Actuators and Target Motion via Fuzzy Integral Sliding Mode Control, IEEE Trans. Fuzzy Syst. (2020).
73 <https://doi.org/10.1109/TFUZZ.2020.2985931>.
- 74 [38] C. Ren, X. Li, X. Yang, S. Ma, Extended state observer-based sliding mode control of an omnidirectional mobile robot
75 with friction compensation, IEEE Trans. Ind. Electron. 66 (12) (2019) 9480-9489.

- 1 <https://doi.org/10.1109/TIE.2019.2892678>.
- 2 [39] E. Cruz-Zavala, J. A. Moreno, Homogeneous high order sliding mode design: a Lyapunov approach, *Automatica* 80 (2017) 232-238. <https://doi.org/10.1016/j.automatica.2017.02.039>.
- 3 [40] Y. Yan, S. Yu, X. Yu, Quantized super-twisting algorithm based sliding mode control, *Automatica* 105 (2019) 43-48. <https://doi.org/10.1016/j.automatica.2019.03.002>.
- 4 [41] X. Tu, J. Gai, L. Tang, Robust navigation control of a 4WD/4WS agricultural robotic vehicle, *Comput. Electron. Agric.* 164 (2019) 104892. <https://doi.org/10.1016/j.compag.2019.104892>.
- 5 [42] R. Khan, F. M. Malik, A. Raza, N. Mazhar, Comprehensive study of skid-steer wheeled mobile robots: development and challenges, *Ind Robot: Int J. Robot. Research Appl.* 48 (1) (2020) 142-156. <https://doi.org/10.1108/IR-04-2020-0082>.
- 6 [43] J. Hu, Y. Han, J. Chen, Integrated control of direct yaw moment control and active suspension system for 4wd vehicles, *Mechanics* 23 (3) (2017) 412-424. <https://doi.org/10.5755/j01.mech.23.3.18481>.
- 7 [44] X. Z. Jin, Y. X. Zhao, H. Wang, Z. Zhao, X. P. Dong, Adaptive fault-tolerant control of mobile robots with actuator faults and unknown parameters, *IET Control Theory Appl.* 13(11) (2019) 1665-1672. <https://doi.org/10.1049/iet-cta.2018.5492>.
- 8 [45] R. Seeber, M. Reichhartinger, Conditioned Super-Twisting Algorithm for systems with saturated control action, *Automatica* 116 (2020) 108921, 2020. <https://doi.org/10.1016/j.automatica.2020.108921>.
- 9 [46] U. Pérez-Ventura, L. Fridman, Design of super-twisting control gains: A describing function based methodology, *Automatica* 99 (2019) 175-180. 2019. <https://doi.org/10.1016/j.automatica.2018.10.023>.
- 10 [47] F. Zhang, P. Huang, Fuzzy-based Adaptive Super-Twisting Sliding-Mode Control for a Maneuverable Tethered Space Net Robot, *IEEE Trans. Fuzzy Syst.* (2020) published online. <https://doi.org/10.1109/TFUZZ.2020.2985325>.
- 11 [48] T. Chen, L. Chen, X. Xu, Y. Cai, X. Sun, Simultaneous path following and lateral stability control of 4WD-4WS autonomous electric vehicles with actuator saturation, *Adv. Eng. Soft.* 128 (2019) 46-54. <https://doi.org/10.1016/j.advengsoft.2018.07.004>.
- 12 [49] L. Jiang, et al, Decoupled Fractional Super-Twisting Stabilization of Interconnected Mobile Robot Under Harsh Terrain Conditions, *IEEE Trans. Ind. Electron.* (2021). <https://doi.org/10.1109/TIE.2021.3111557>.
- 13 [50] B. Li, H. Du, W. Li, B. Zhang, Integrated dynamics control and energy efficiency optimization for overactuated electric vehicles, *Asian J. Control* 20 (5) (2018) 1952-1966. <https://doi.org/10.1002/asjc.1686>.
- 14 [51] H. Zhang, W. Z. Zhao, Decoupling control of steering and driving system for in-wheel-motor-drive electric vehicle, *Mechanical Syst. Signal Proce.* 101 (2018) 389-404. <https://doi.org/10.1016/j.ymssp.2017.08.042>.
- 15 [52] L. Jiang et al., Anti-Disturbance Direct Yaw Moment Control of a Four-Wheeled Autonomous Mobile Robot, *IEEE Access* 8 (2020) 174654-174666. <https://doi.org/10.1109/ACCESS.2020.3025575>.
- 16 [53] L. Zhai, T. Sun, J. Wang, Electronic stability control based on motor driving and braking torque distribution for a four in-wheel motor drive electric vehicle, *IEEE Trans. Veh. Technol.* 65 (6) (2016) 4726-4739. <https://doi.org/10.1109/TVT.2016.2526663>.
- 17 [54] J. A. Moreno, M. Osorio, Strict Lyapunov Functions for the Super-Twisting Algorithm, *IEEE Trans. Autom. Control* 57 (4) (2012) 1035-1040. <https://doi.org/10.1109/TAC.2012.2186179>.
- 18 [55] Y. B. Shtessel, J. A. Moreno, F. Plestan, L. M. Fridman, A. S. Poznyak, Super-twisting adaptive sliding mode control: A Lyapunov design, in: *Proceedings of 49th IEEE Conference Decision Control (CDC)*, IEEE Atlanta, GA, USA, 2010, pp. 5109-5113. <https://doi.org/10.1109/CDC.2010.5717908>.
- 19 [56] H. Obeid, L. Fridman, S. Laghrouche, M. Harmouche, M. A. Golkani, Adaptation of Levant's differentiator based on barrier function, *Int. J. Control* 91 (9) (2018) 2019-2027. <https://doi.org/10.1080/00207179.2017.1406149>.
- 20 [57] H. Obeid, S. Laghrouche, L. Fridman, Y. Chitour, M. Harmouche, Barrier function-Based Adaptive Gain Super-Twisting Controller, *IEEE Trans. Autom. Control* 65 (11) (2020). <https://doi.org/10.1109/TAC.2020.2974390>.
- 21 [58] M. Rubagotti, D. Raimondo, A. Ferrara, L. Magni, Robust model predictive control with integral sliding mode in continuous-time sampled-data nonlinear systems, *IEEE Trans. Autom. Control* 56 (3) (2010) 556-570. <https://doi.org/10.1109/TAC.2010.2074590>.
- 22 [59] Y. Huangfu, L. Guo, R. Ma, F. Gao, An Advanced Robust Noise Suppression Control of Bidirectional DC-DC Converter for Fuel Cell Electric Vehicle, *IEEE Trans. Trans. Electrific.* 5 (4) (2019) 1268-1278. <https://doi.org/10.1109/TTE.2019.2943895>.
- 23 [60] L. Magni, R. Scattolini, Model predictive control of continuous-time nonlinear systems with piecewise constant control, *IEEE Trans. Autom. Control* 49 (6) (2004) 900-906. <https://doi.org/10.1109/TAC.2004.829595>.
- 24 [61] D. Cole, A. Pick, A. Odhams, Predictive and linear quadratic methods for potential application to modelling driver steering control, *Vehicle Syst. Dyn.* 44 (3) (2006) 259-284. <https://doi.org/10.1080/00423110500260159>.
- 25 [62] T. Johansen, I. Petersen, O. Slupphaug, Explicit sub-optimal linear quadratic regulation with state and input constraints, *Automatica* 38 (7) (2002) 1099-1111. [https://doi.org/10.1016/S0005-1098\(02\)00004-3](https://doi.org/10.1016/S0005-1098(02)00004-3).
- 26 [63] J. Zhang, T. Shen, Real-time fuel economy optimization with nonlinear MPC for PHEVs, *IEEE Trans. Control Syst. Technol.* 24 (6) (2016) 2167-2175. <https://doi.org/10.1109/TCST.2016.2517130>.
- 27 [64] M. Kiran, H. Hakli, M. Gunduz, H. Uguz, Artificial bee colony algorithm with variable search strategy for continuous optimization, *Inf. Sci.* 300 (2015) 140-157. <https://doi.org/10.1016/j.ins.2014.12.043>.
- 28 [65] J. Meng, et al., A safe and efficient LIDAR-based navigation system for 4WS4WD mobile manipulators in manufacturing plants, *Meas. Sci. Technol.* 32 (4) (2021) 045203. <https://doi.org/10.1088/1361-6501/abce71>.
- 29 [66] J. Meng, et al., Efficient and Reliable LiDAR-based Global Localization of Mobile Robots Using Multi-scale/resolution Maps, *IEEE Trans. Instrum. Meas.* (2021) published online. <https://doi.org/10.1109/TIM.2021.3093933>.
- 30 [67] R. Szczepanski, T. Tarczewski, L. M. Grzesiak, Adaptive state feedback speed controller for PMSM based on Artificial Bee Colony algorithm, *Appl. Soft. Comput.* 83 (2019) 105644. <https://doi.org/10.1016/j.asoc.2019.105644>.